2023

Analysis of Multi-Drug Resistant Mycobacterium tuberculosis Using Split Deoxyribozymes

Abryana Fergus
University of Central Florida

ANALYSIS OF MULTI-DRUG RESISTANT *MYCOBACTERIUM TUBERCULOSIS* USING SPLIT DEOXYRIBOZYMES

BY

ABRYANA FERGUS

B.S. UNIVERSITY OF CENTRAL FLORIDA, 2020

A thesis submitted in partial fulfillment of the requirements
for the degree of Master of Sciences
in the Department of Chemistry
in the College of Sciences
at the University of Central Florida
Orlando, Florida

SPRING 2023

ABSTRACT

Globally, tuberculosis, a disease caused by the species of *Mycobacterium tuberculosis* (Mtb) complex, stands as a leading cause of death from a single infectious agent. Even though antituberculous drugs are available, treatment is challenging due to antibiotic resistance associated with point mutations in the bacterial genome. Resistance to the first-line antibiotics – rifampin and isoniazid – results in multidrug-resistant tuberculosis (MDR) requiring a more complicated treatment regimen. Timely and accurate identification of drug-resistant TB cases can help prescribe the most effective treatment and prevent the spread of infection.

This research aims to develop an assay to discern multi-drug resistant forms of tuberculosis using a molecular assay based on split deoxyribozyme hybridization probes. For the probe design, a catalytic core of an RNA-cleaving deoxyribozyme is split into two parts, with each part elongated with a target-recognizing fragment ("arm"). In the presence of a fully complementary nucleic acid target, but not the one containing point mutations, the catalytic core of the deoxyribozyme can be re-formed due to the assembling of the target-probe complex, which recognizes and allows cleavage of a fluorophore- and quencher-labeled signal reporter, thereby ensuring increase in fluorescence in a target-dependent manner. The target-binding arms of the probes were optimized in terms of the signal-to-background ratio and selectivity of target recognition using synthetic targets corresponding to the fragments of the *katG* and *rpoB* genes with point-mutation sites implicated in the resistance to isoniazid and rifampin, respectively. The optimized probe sequences were used to interrogate the targets obtained by amplifying the

correspondent fragments of the Mtb genes using Linear- After-The-Exponential (LATE) PCR, which allows efficient synthesis of a single-stranded amplicon.

The signal triggered by cognate targets can be read using a portable fluorometer, which eliminates the need to use a sophisticated real-time PCR instrument for the assay. The success of the split deoxyribozyme assay can establish an affordable and user-friendly molecular diagnostic assay where a sample can be amplified and analyzed in a single tube.

Dedicated to my great-grandmother Henrietta Jarrett, your love, light, and legacy lives on.

ACKNOWLEDGMENTS

I would like to thank everyone who has supported me throughout the last 2.5 years. I have had great doubts within myself, my work, and my future but my support system has kept the fire alive the whole time. I would like to extend a special thanks to my advisor Dr. Yulia Gerasimova who has provided me with unrelenting guidance and support.

TABLE OF CONTENTS

LIST OF FIGURES

LIST OF TABLES

LIST OF ABBREVIATIONS AND ACRONYMS

A – Adenine

aPCR – Asymmetric Polymerase Chain Reaction

BCG – Bacillus Calmette–Guérin

BSL-3 – Biosafety Level 3

C – Cytosine

DMSO – Dimethyl sulfoxide

DNA – Deoxyribonucleic Acid

dNTP – Deoxyribonucleotide Triphosphate

dsDNA – Double Stranded Deoxyribonucleic Acid

DST – Drug-Susceptibility Testing

Dz – Deoxyribozyme

G – Guanine

FP – Forward Primer

HEPES – N-(2-Hydroxyethyl)piperazine-N'-(2-ethanesulfonic acid)

HVR – Hypervariable Region

INH – Isoniazid

L – Limiting Primer

LATE-PCR – Linear-After-The-Exponential Polymerase Chain Reaction

LPA – Line Probe Assay

LOD – Limit of Detection

MB – Molecular Beacon

MDR – Multi-drug Resistant

MDR-TB – Multi-drug Resistant Tuberculosis

MTB – *Mycobacterium tuberculosis*

MTC - *Mycobacterium tuberculosis* Complex

MUT – Mutant

NAD-INH – Nicotinamide Adenine Dinucleotide – Isoniazid

NT - Nucleotide

NTC – No Template Control

PCR – Polymerase Chain Reaction

qPCR – Quantitative Polymerase Chain Reaction

RRDR – *rpoB* Resistance Determining Region

RIF – Rifampin

RNA – Ribonucleic Acid

RP – Reverse Primer

S/B – Signal-to-Background Ratio

sDz – Split Deoxyribozyme

ssDNA – Single Stranded Deoxyribonucleic Acid

SELEX – Systematic Evolution of Ligands by Exponential Enrichment

SNP – Single Nucleotide Polymorphism

T – Thymine

T_m – Melting Temperature

T_m^L – Limiting Primer Melting Temperature

T_m^X – Excess Primer Melting Temperature

TB – Tuberculosis

TR – Texas Red

U – Uracil

ULR – Ultra Low Range

X – Excess Primer

WHO – World Health Organization

WT – Wildtype

λ_{max} – Lambda Max

CHAPTER ONE: INTRODUCTION

1.1 – Tuberculosis: Worldwide Impact and Drug Resistance

Tuberculosis (TB), a disease caused by *Mycobacterium tuberculosis* (Mtb) and other mycobacterial species classified as the Mtb complex (MTC), currently stands as the leading cause of death globally from a single infectious agent.[1] TB is spread from the lungs through the air when an infected person coughs or speaks, and the bacteria are inhaled by people nearby. The bacteria begins to grow after it settles into the lungs and has the ability to enter the bloodstream to move into other organs.[2] In 2021, 6.4 million people were newly diagnosed with TB according to the 2022 Global Tuberculosis Report published by the World Health Organization (WHO).[1] TB presents itself as a persistent public health threat that appears predominantly in low-income, developing areas such as South-East Asia, Africa, and Western Pacific areas. Despite available treatment methods, TB continues to be a challenge partially due to its multi-drug resistance.

Multi-drug resistant TB (MDR-TB) are forms of tuberculosis that are resistant to the front-line drugs isoniazid (INH) and rifampin (RIF).[3] These cases call for second-line drugs that are often costly, riddled with side effects, and have decreased success rates. Studies show that in countries with a high occurrence of TB, INH resistance paired with RIF susceptibility is common.[4] Contrarily, RIF resistance is often co-found with INH resistance, thus making RIF resistance a surrogate marker for MDR-TB.[4] Currently, 3.4 % of new TB cases display multi-drug resistance. 1.5% of TB patients develop MDR-TB due to inadequate treatment regimen, while 0.4% of TB patients in remission develop MDR-TB through reinfection[3, 5]. The WHO attempts to combat the spread of TB and increased drug resistance by means of early detection.

Presently, bacteriological confirmation of TB is required when testing for MDR through the means of bacterial culture, molecular systems, or sequencing technologies.[1] However, these diagnostic methods are timely, expensive, and require special expertise and instrumentation.

1.2 – Current Diagnostic Methods

Culture-based drug-susceptibility testing (DST) stands as the current gold standard for MDR-TB detection.[4] A culture isolated from a clinical specimen is usually grown for about 4 weeks, and then it is exposed to anti-TB drugs on a growth medium. For improved efficiency, direct DST is a method used to save time by directly inoculating a drug-containing medium with a clinical specimen sample. Direct inoculation reduces the turnaround time to 15-25 days and shows comparable accuracy in detection to that of a conventional culture-based DST.[6] Both techniques are low-cost and reliable MDR-TB detection methods, however, they exhibit slow turnaround times and require expert knowledge of bacterial culture techniques, as well as the settings certified to work with BSL3 organisms.

In an attempt to improve early MDR-TB detection, line probe assay technology (LPA) was evaluated as a rapid testing method. LPAs rely on the reverse hybridization of DNA amplicon with immobilized probes (Figure 1).[7] Probes are designed to target common Mtb mutation sites, and drug resistance is detected by Mtb amplicon binding to mutant-specific probes or the lack of binding to wild-type probes.[7] In the event of hybridization, a colored band is developed on the test strip at the site of binding (Figure 1B). In 2008, LPAs were approved by the WHO for rapid detection of MDR-TB, showcasing it is effective in testing culture isolates

and direct testing of smear microscopy samples.[7] In clinical studies, LPAs showcased the ability to detect RIF resistance with a sensitivity of 95.8% and specificity of 98.4%. In INH resistance detection, LPAs showed a sensitivity of 94.5% and 99.3% specificity.[4] Despite the success of the assay, the LPA method has some limitations. While LPAs detect the most common mutations in resistant strains, it fails to detect mutations outside of the regions covered by the test and can require phenotypic DST. Additionally, LPA is less efficient when detecting samples that contain both drug-susceptible and drug-resistant bacteria.[7]

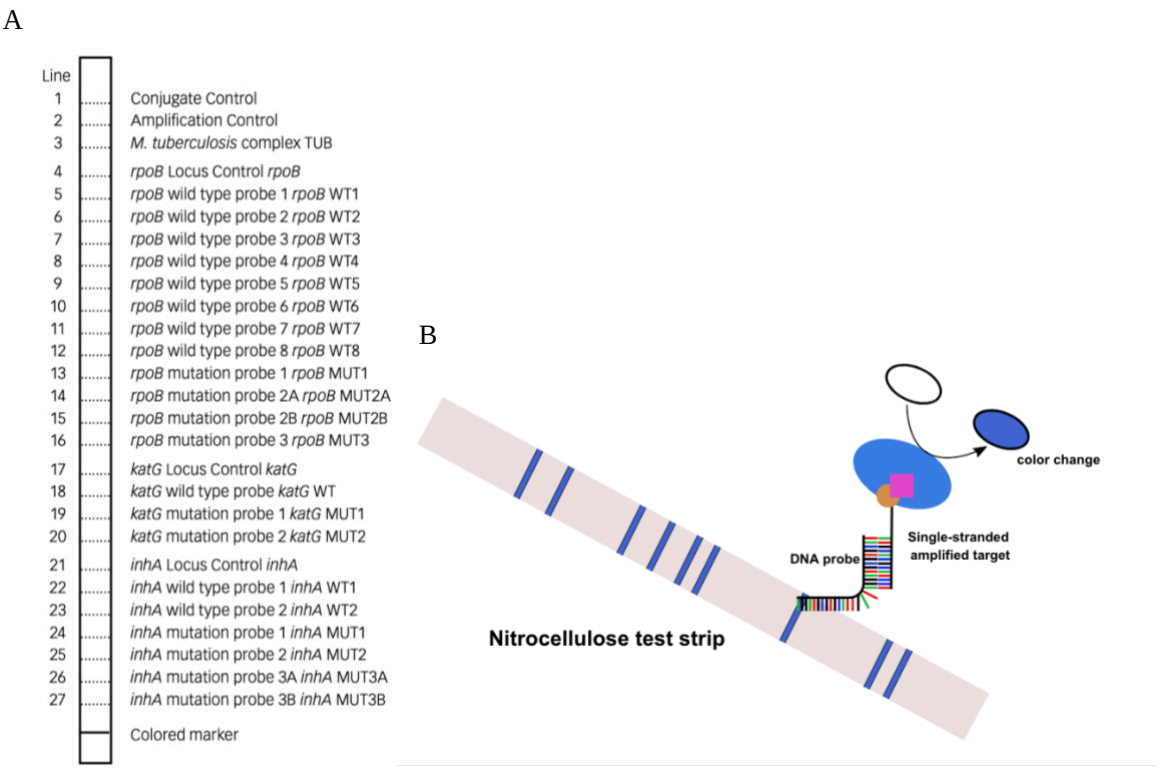

Figure 1: A. GenoType MTBDRplus V2 Mtb Line probe assay.[7] B. Schematic of LPA assay mechanism.

In 2011, the WHO endorsed a revolutionary diagnostic system, the Xpert MTB/RIF, a real-time nucleic acid amplification assay that employs molecular beacons.[8] Molecular beacon probes are fluorescently labeled single-stranded oligonucleotides that fluoresce upon

hybridization to their complementary target. The structure contains a stem-loop, which acts as the hybridization location of the target sequence (Figure 2).[9] These probes are often used for pathogen detection, genome analysis, and amplification monitoring during PCR.[9] The Xpert MTB/XDR system includes a cartridge for sample processing, bacterial lysis, and nucleic acid capturing and, therefore, provides detection directly from clinical samples and offers a quick turnaround time of 3 hours, compared to LPA methods, which can take 2-3 days.[4, 8] This assay can reliably detect 90% of TB cases, however, it requires costly instrumentation and the purchase of single-use cartridges.[8]

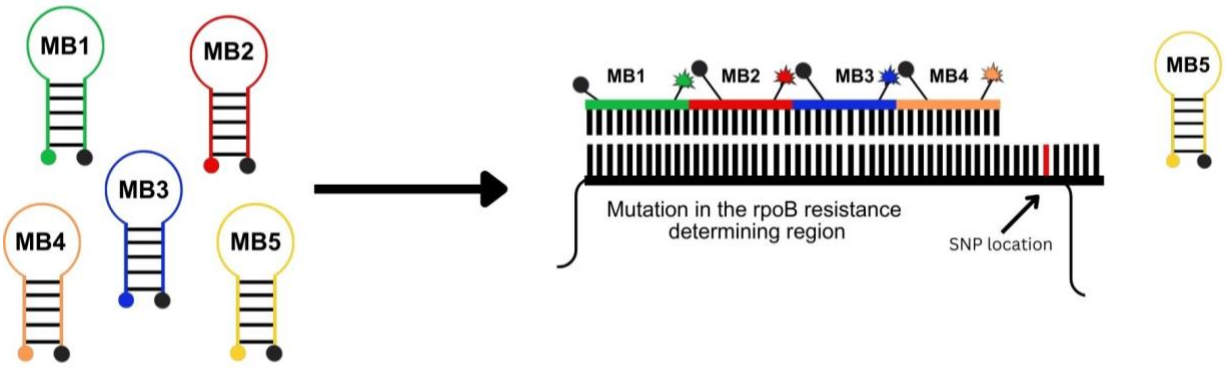

Figure 2: Scheme of molecular beacon (MB) probe technologies used in the Xpert MTB/XDR assay. Multiple molecular beacons can be used to flank a target sequence. The absence of signal from a single MB (e.g. MB5) can signify RIF resistance.[10]

1.3 – Genes of Interest

Drug resistance can be attributed to single nucleotide polymorphisms (SNPs) located in the Mtb genome. SNPs are substitutions of a single nucleotide in a gene and are often found in a substantial portion of the MDR-TB bacterial population. Multidrug resistance in Mtb is often associated with the genes *katG* and *rpoB*, where the presence of SNPs in these regions inhibits the antituberculous functions of INH and RIF, respectively.

Resistance to INH is conferred when a SNP is located at codon 315, where a G is changed to a C, resultantly changing the amino acid from a serine to a threonine once transcribed. (Figure 3). INH is a prodrug that requires activation by the homodimer enzyme, catalase-peroxidase, which is encoded within the *katG* gene. Upon activation, INH interacts with NADH in the enzyme's active site to produce an NAD-INH complex.[11] The complex is a recognized inhibitor of InhA, an enzyme that facilitates the biosynthesis of mycolic acid, a vital component in the Mtb cell wall.[12] In the case of a mutated *katG* gene catalase-peroxidase is no longer functional, and INH is not converted to its active form (Figure 4). Isoniazid resistance can also be conferred due to mutations occurring at the -15 position in the promoter region of the *inhA* gene. Mutations in this region lead to an overexpression of the protein inhA which facilitates the titration of INH, requiring higher doses of the drug for total inhibition.[13, 14] This mutation is often associated with low levels of resistance to INH, and is present in 19% of isoniazid-resistant clinical samples.[14]

Figure 3: Codons 298 – 316 of the *katG* sequence showcasing 315 codon and SNP frequency. 75% - 90% of INH-resistant clinical isolates contain SNPs located in codon 315.[15]

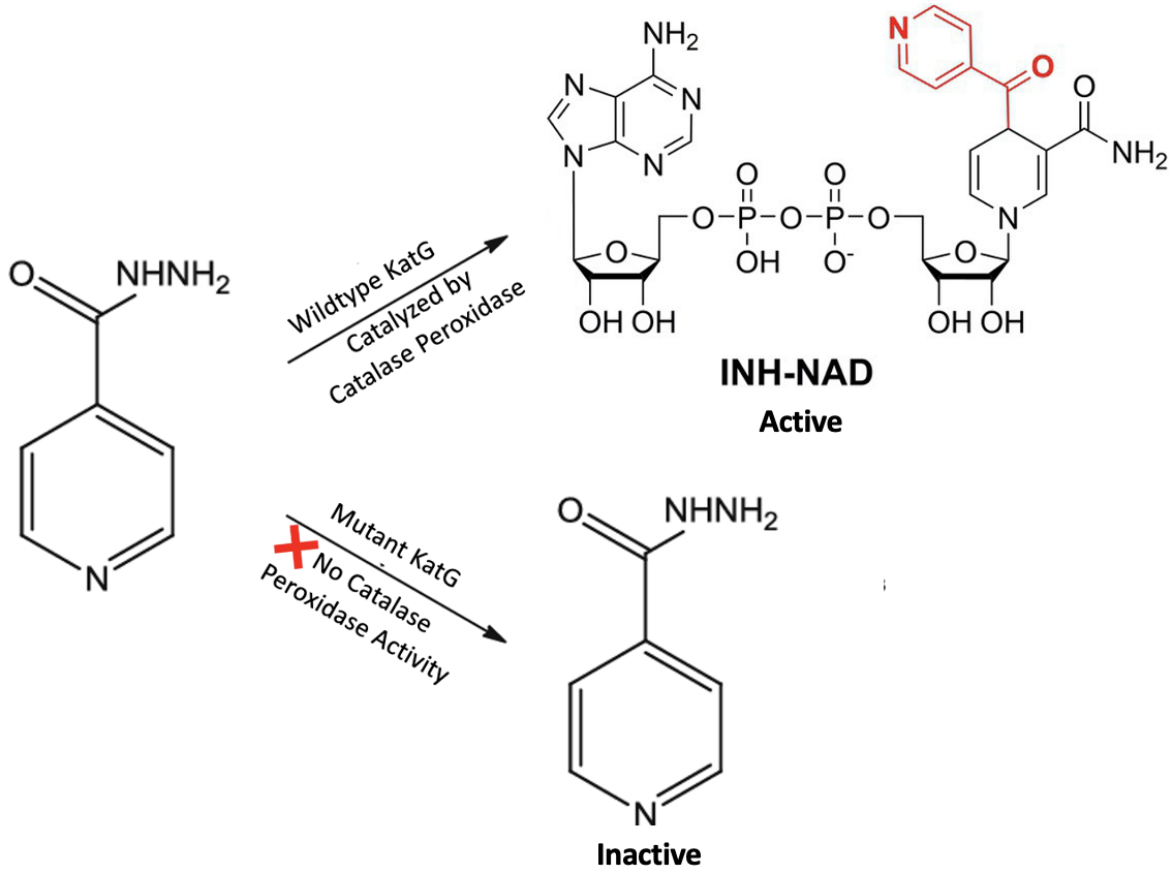

Figure 4: Schematic of catalase-peroxidase catalyzing INH to its active form. Mutations in the katG leads to the inactivation of catalase-peroxidase and confer resistance.

RIF targets the active site of bacterial RNA polymerase, the enzyme responsible for the transcription of RNA. Amino acid substitutions caused by mutations in the *rpoB* gene lowers the affinity of RIF to RNA polymerase and prevents the drug from binding (Figure 5).[16] Drug resistance can be conferred by SNPs at any position in the 81-base pair RIF resistance determining region (RRDR) of the *rpoB* gene (Figure 6).[12, 17] Codons 526 and 531 are extensively studied and display a high incidence of SNPs where nucleotide C is replaced with a T or G.[18]

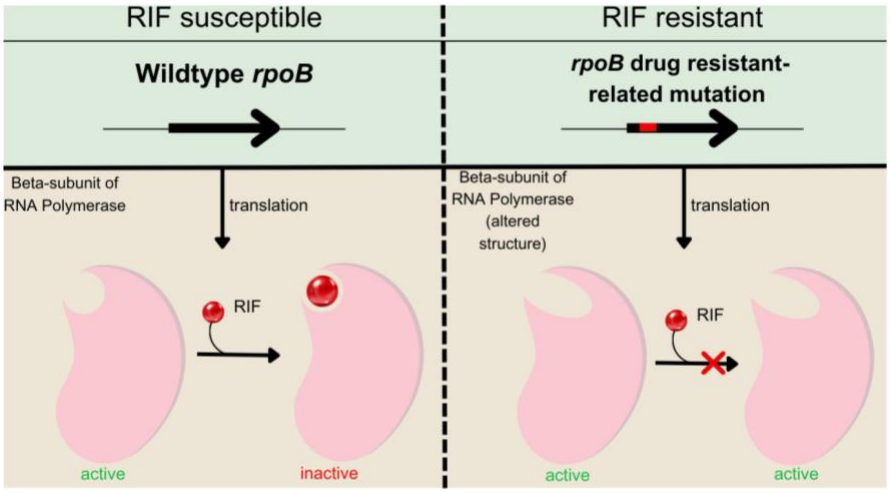

Figure 5: *rpoB* gene translates the B-subunit of bacterial RNA polymerase, changes in the gene cause changes in the polymerase structure and RIF resistance.[19]

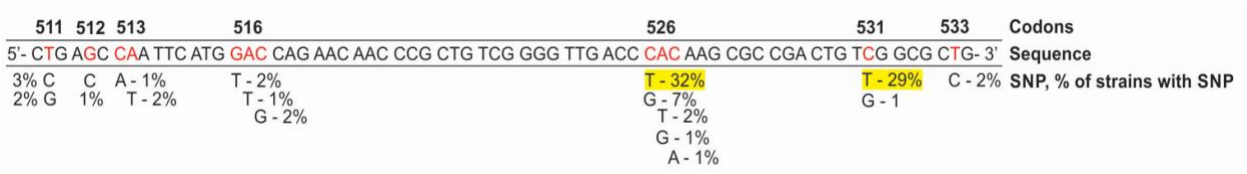

Figure 6: Region of the RDRR in *rpoB* showcasing SNP hotspots and frequencies. C to T transversions at codon 526 is seen in 32% of RIF-resistant Mtb.

1.4 – Deoxyribozymes

Most biological functions of deoxyribonucleic acid (DNA) are associated with its ability to form a double-stranded helix. At the same time, single-stranded DNA (ssDNA) fragments can fold into alternative secondary structures that have the potential for catalytic activity.[20] In 1997, Santoro and Joyce used *in vitro* selection using Systematic Evolution of Ligands by Exponential Enrichment (SELEX) technique to isolate the first deoxyribozyme (Dz) or DNAzyme, a ssDNA molecule that possess site-specific RNA cleaving capabilities.[21] The introduction of this innovative technique widened the possibilities to facilitate biochemical reactions and develop bioanalytical tools. Dz has proven to be a stable, economical, and powerful sensor for a variety of analytes due to its ability for catalytical signal amplification.[22]

Catalytic signal amplification is facilitated by the catalytic core, 10-23, a DNAzyme with extraordinary cleavage activity and specificity.[23] 10-23 is the most comprehensively studied RNA-cleaving DNAzyme and is composed of a 15-nucleotide catalytic loop that is flanked by two substrate binding arms. The core is advantageous because the arms can be customized to cleave various RNA targets, however, it requires two ribonucleotides to aid cleavage.[22] The cleavage site is nestled between the ribonucleotide sequence R-Y, where R is a purine and Y is a pyrimidine (Figure 7). In a study conducted by Cairns et al. it was concluded that the diribonucleotide sequences AU and GU were most susceptible to enzymatic cleavage.[26] For cleavage catalysis, 10-23 requires divalent metal ions such as Ca^{2+} or Mg^{2+}.[24,27] It is proposed that at the cleavage site, the metal ion acts as a general base by assisting the deprotonation of the 2'-hydroxyl but also doubles as a Lewis acid, coordinating the 2' hydroxyl to increase the acidity. This produces a 2' oxyanion intermediate that performs a nucleophilic attack on the neighboring phosphate (Figure 7).[28] This coordination is important because it ensures the stability of the transition states in the reaction and supports the folding of the Dz into an active conformation.[27]

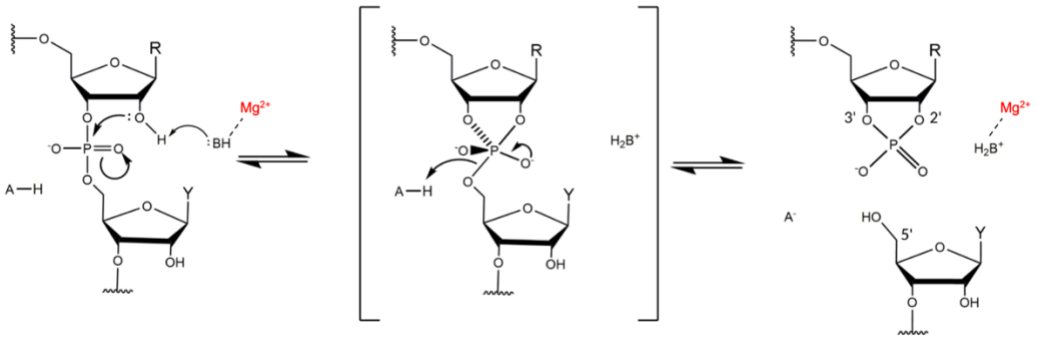

Figure 7: Proposed mechanism of 10-23 DNAzyme catalytic core.[28] Studies show increased cleavage activity when the cleavage sites are diribonucleotides AU & GU (AU = GU ≥ GC >> AC). [26]

Split deoxyribozymes (sDz), also known as multicomponent nucleic acid enzymes (MNAzymes), introduce a unique approach to molecular interrogations due to their multi-component design.[29] These sensors are comprised of two parts, Dza and Dzb, which hybridize with a complementary nucleic acid sequence (target or assembly facilitator) and activate a catalytic core that facilitates phosphodiester cleavage between a reporter/quencher labeled substrate, consequently producing a fluorescent signal (Figure 8). Once ribonucleotides in the substrate strand have been cleaved the affinity for the Dz complex is decreased and replaced by a new uncleaved substrate strand. This showcases how sDz operates like a true enzyme due to its ability for multiple turnovers (Figure 8).[29] Split deoxyribozymes possess the ability to bind to different target sequences while conserving the sequence of the catalytic core, further showing its universal applications.

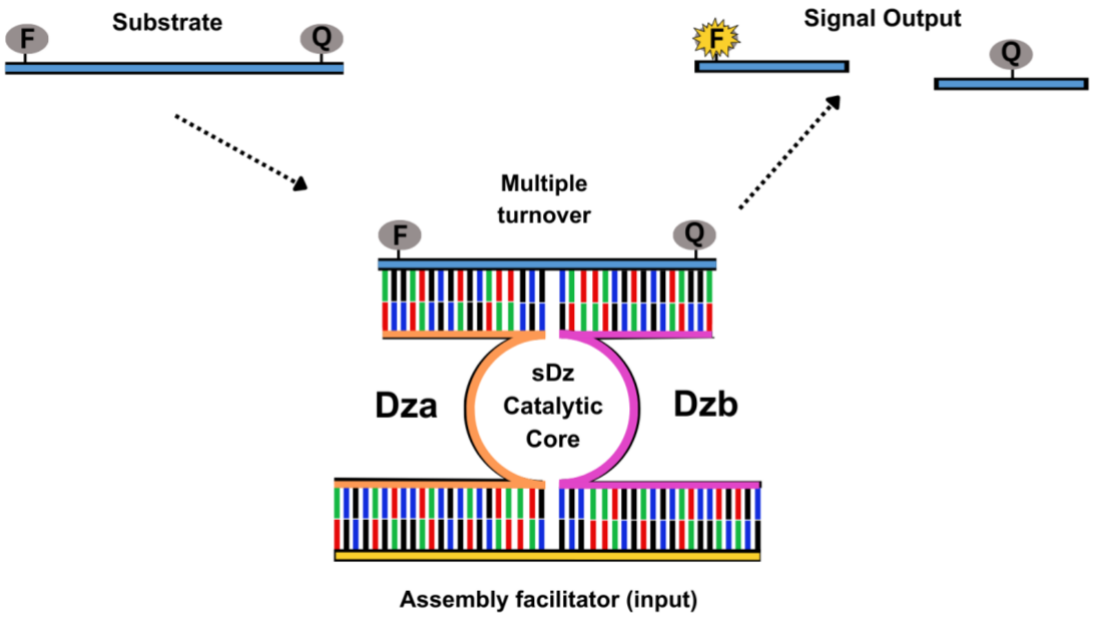

Figure 8: Mechanism of split deoxyribozyme assembly and substrate cleavage to produce a fluorescent output in the presence of a complementary target (assembly facilitator).[29]

sDz displays higher selectivity than conventional probes such as molecular beacons due to its split character. Indeed, it allows allocating different probe's functions (e.g. affinity to the target, selectivity of target recognition, accessing the probe-binding fragment of the target) to different probe's components and independent optimization of the components for optimal probe performance. For example, to increase the stability of the probe-target complex for high signal output, one target-binding fragment can be elongated. This can also help unwind the secondary/tertiary structure of the target. At the same time, to preserve high selectivity of the probe-target recognition, another target-binding arm can be designed relatively short and, therefore, sensitive to mispairings down to a single nucleotide (Figure 9).[22] Additional functionalities (e.g. additional target-binding/unwinding fragments, substrate-attracting functionalities, etc.) can be introduced to further perfect the analytic system. [22]

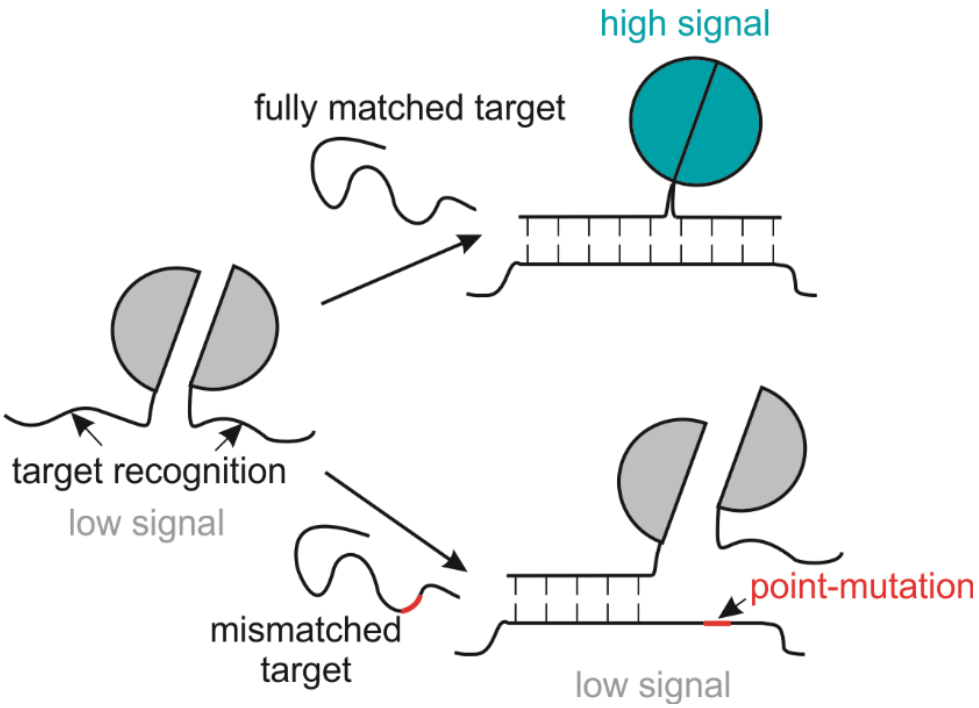

Figure 9: General scheme depicting how the generation of signal from the split hybridization probes is target-dependent. In the presence of a mismatch, the catalytic core is not formed resulting in low signal output.

1.5 – DNA Amplification

The development of techniques for the *in vitro* amplification of DNA and RNA sequences revolutionized molecular biology. Polymerase Chain Reaction (PCR) is a technique used to rapidly produce millions of copies of a specific segment of DNA or RNA using a thermophilic DNA polymerase, dNTPs, and a pair of oligonucleotide primers. It follows a cycling process that involves three steps (Figure 9).[30] The initial step uses high temperatures (95-98°C) to promote the denaturation of the double-stranded DNA (dsDNA) template. Then, the temperature of the reaction is lowered to be about 2-5 °C lower than the melting temperature

(T_m) of the primers to facilitate the next step, annealing, which is the binding of the primers to the complementary fragments of the separated ssDNA strands of the template. The final step, extension, occurs when the reaction temperature is increased to the optimal temperature for the activity of DNA polymerase to enable the elongation of the primers. This cycle is repeated for 30-35 cycles and theoretically produces double the amount of DNA from the previous cycle.[30]

Taq polymerase, an enzyme isolated from the heat-tolerant organism *Thermus aquaticus* is often used as a thermostable polymerase due to its ability to remain stable at high temperatures in contrast to the behavior of traditional enzymes at elevated temperatures.[31] After amplification, the amplicon can be visualized using a polyacrylamide or agarose gel electrophoresis.[30]

Alternatively, amplified targets can be quantified using quantitative PCR (qPCR) methods. qPCR utilizes a fluorescent probe to monitor the quantity of amplified products in real time. Fluorescence intensity is recorded after each cycle and the signal is representative of the amount of DNA amplicon present in the sample.[32]

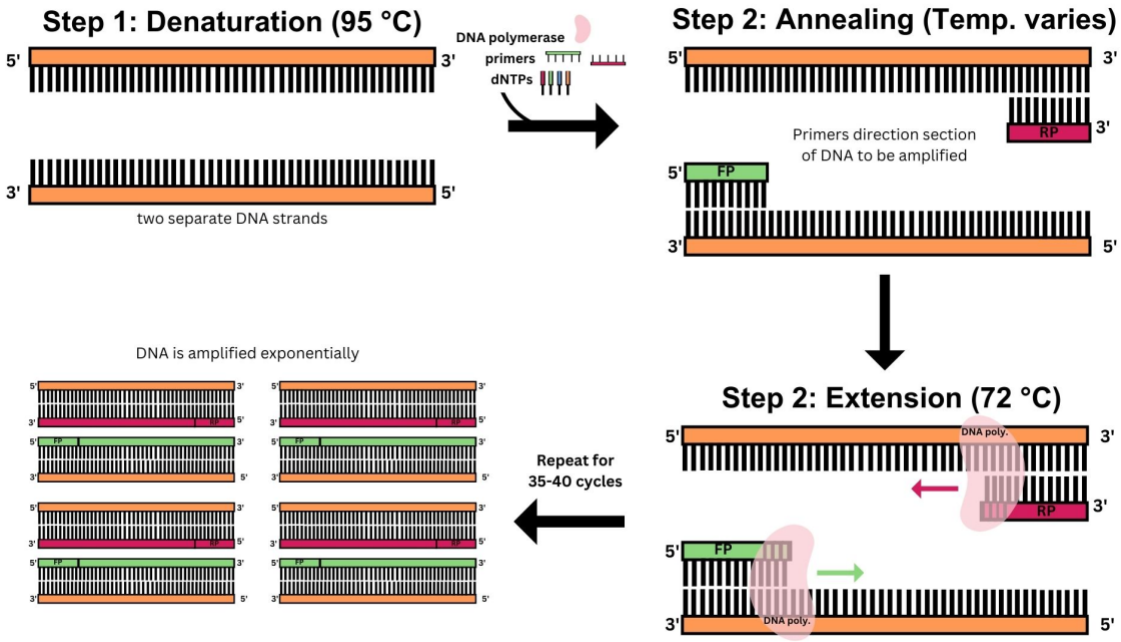

Figure 10: Schematic of polymerase chain reaction (PCR) cycles.[33]

Asymmetric PCR (aPCR) is performed when unequal molar concentrations of primers are used to predominantly generate a ssDNA amplicon for sequencing and use in microarrays.[34] The primer corresponding to the sequence of the unwanted strand is used in a lower concentration (limiting (L) primer) than the primer defining the targeted strand of the DNA template (excess (X) primer). However, amplification efficiencies associated with traditional aPCR methods are greatly variable and require thorough optimization to maximize single-stranded products while reducing the assembly of non-specific products. Lowering the concentration of one primer while using the traditional symmetric PCR method lowers the efficiency of the reaction due to the reaction's dependence on the annealing temperature. Annealing temperatures are determined by the melting temperature (T_m) of the primers and are traditionally set to three degrees less than the primer with the lowest T_m. [35] As the concentration of primer is decreased, the T_m also decreases therefore making it difficult to select an annealing

temperature that is conducive to the binding of both primers. Choosing an annealing temperature that only satisfies the binding of the limiting primer increases the probability of a nonspecific product caused by the mispriming of the excess primer.[36]

Implementation of LATE-PCR or Linear-After-The-Exponential PCR circumvents this issue by using primers that are intentionally designed to be used at unequal concentrations by extending the limiting primer sequence to compensate for the differences in T_m.[36] This method requires the addition of nucleotides to the limiting primer such that T_m^L is equal or greater than T_m^X (i.e., $T_m^L - T_m^X \geq 0$). Amplification via LATE-PCR begins in an exponential phase analogous to that of symmetric amplification. When the limiting primer is consumed, the reaction enters its linear phase where ssDNA amplicon is formed.[36]

1.6 – Research Objective

The study aims to expand molecular tools available for DST for TB patients by developing and optimizing split deoxyribozyme probes targeting fragments of the *katG* and *rpoB* genes with point mutations associated with INH and RIF resistance, respectively. The sDz probe serves as a cost-effective tool that can be edited and optimized to a variety of target sequences, and, therefore, is promising for an affordable, adaptable, user-friendly molecular diagnostic assay.

CHAPTER TWO: METHODOLOGY

2.1 – Materials and Instrumentation

All unmodified oligonucleotides were synthesized by Integrated DNA Technologies, Inc. (Coralville, IA). The fluorogenic substrates were synthesized by TriLink BioTechnologies, Inc. (San Diego, CA). PCR reactions were performed using the Phusion Flash High-Fidelity PCR Master Mix from ThermoFisher Scientific (Waltham, MA). *katG* and *rpoB* gene fragments were amplified from total DNA isolated from *Mycobacterium bovis* BCG, kindly provided by Dr. Rohde (UCF, BSBS). Fluorescent spectra were obtained using a Cary Eclipse Fluorescence Spectrophotometer (Agilent Technologies, Inc.), with the help of a Starna Cell 50μL sub-micro fluorimeter quartz cuvette. Agarose gels were prepared using Lonza SeaKem ® LE agarose powder. Gel analysis was performed using Owl EasyCast B2 Mini Gel Electrophoresis System (ThermoFisher Scientific). All statistical analysis was performed using Microsoft Excel Data Analysis Toolpak.

2.2 – Polymerase Chain Reaction (PCR)

Total DNA isolated from *Mycobacterium bovis* BCG was used as a template for PCR. Each sample (20 μL) contained 10 μL 2X Flash Phusion PCR Master Mix and 1 μL of the 10 μM forward primer and 0.5 μM reverse primer each in the absence or presence of 0.75 ng/μL DNA template. Samples were placed in the BioRad C1000 thermocycler and set to the following conditions: initial denaturation at 98°C for 20 s, followed by 35 cycles of denaturation at 98°C for 5 s, annealing at 62°C or 57°C (to amplify fragments of the *katG* and *rpoB* genes, respectively) for 10 s, extension at 72°C for 5 s and a final extension at 72°C for 1 min.

2.3 – Split Deoxyribozyme Assay

A reaction buffer contained 50 mM HEPES-NaOH (pH 7.4), 50 mM $MgCl_2$, 20 mM KCl, 120 mM NaCl, 0.03% Triton-X100, and 1% DMSO. The efficacy of the split deoxyribozyme probes was tested using samples (60 μL) containing 200 nM fluorogenic substrate, 30 nM Dza and 30 nM Dzb, either synthetic DNA target (1 nM or 10 nM) or PCR amplicon (10% v/v) in the reaction buffer. For the blank control, a sample containing the fluorogenic substrate and Dza and Dzb in the absence of targets was used. When PCR amplicons were tested, another negative control containing PCR no-target control (10% v/v) was used. Samples were vortexed, spun down, and incubated at 54°C for 60 minutes. After incubation, 50 μLs of the sample were transferred to a quartz cuvette and excited at 485 nm or 595 nm for the *katG*- or *rpoB*-specific sDz probes, respectively, using the Agilent Cary Eclipse Fluorescence Spectrophotometer. The emission spectra were collected, and the intensity at 517 nm or 612 nm for the *katG*- or *rpoB*-specific sDz probes, respectively, was recorded.

2.4 – Gel Electrophoresis Analysis

PCR amplicons were analyzed via 2% agarose gel electrophoresis in 1×TBE buffer. Samples were run at 100V for 45 minutes and visualized by staining the gel with 1×GelRed. The gel images were captured using a Biorad Gel Doc XR+ Imaging System with Image Lab Software.

CHAPTER THREE: DEOXYRIBOZYME ANALYSIS OF *KATG*

3.1 – *katG* Sensor Design

To interrogate the *katG* gene a wildtype (WT) sDz sensor set was designed to target codon 315 where SNPs create drug resistance. The design of this sDz contains a Dza sensor which is referred to as the universal strand due to its ability to bind to the target regardless of the presence of the point mutation. In addition, Dza can be freely edited to manipulate the affinity of the sensors to the target and thus, change the fluorescence signal of the sDz probe. The Dzb sensor is referred to as the selective arm strand, dually because it interacts with the SNP location site, and it is intentionally kept short to reduce binding to a non-specific (e.g. SNP-containing) target. The fluorogenic substrate strand contains FAM, a fluorescent dye, at the C5 position of the second thymine near the 5' end of the substrate and it is excited at 495nm. The fluorescence intensity emitted at 517nm (λ_{max}) is recorded. Black Hole Quencher 1 (BHQ1) is attached to the 3' end of the substrate due to its quenching range between 480 and 580 nm. The substrate is synthesized as a DNA oligonucleotide with 2 ribonucleotides in the center of the sequence that will be cleaved by the catalytic core. The synthetic target was synthesized based on the sequence of the *katG* gene containing codon 315 of the gene.

Table 1: Oligonucleotide sequences used to analyze *katG*

Oligo	Sequence[a]	Length (nts.)
WT Target	GCT GGA AGA GCT CGT ATG GCA CCG GAC CCG GTA AGG ACG CGA T CA CCA GCG GC	53
Mutant Target	GCT GGA AGA GCT CGT ATG GCA CCG GAC CCG GTA AGG ACG CGA TCA CCA CCG GC	53
Dza - 15	TGC CCA GGG A*GG CTA GCT* **ATC GCG TCC TTA CCG**	33
Dza - 19	TGC CCA GGG A*GG CTA GCT* **ATC GCG TCC TTA CCG GTT C**	37
Dza - 21	TGC CCA GGG A*GG CTA GCT* **ATC GCG TCC TTA CCG GTT CCG**	39
Dza - 26	TGC CCA GGG A*GG CTA GCT* **ATC GCG TCC TTA CCG GTT CCG GTG CC**	44
WT Dzb	**GCC GCT GGT G***AC AAC GA*G AGG AAA ACC TT	36
Mutant Dzb	**GCC GGT GGT G***AC AAC GA*G AGG AAA ACC TT	29
Fluorogenic substrate	AAGGTT-(dT-FAM)-TCCTC**gu**CCCTGGGCA-(BHQ1)	22
katG FP	ATG GCC ATG AAC GAC GTC	18
katG RP	CTC CCA CTC GTA GCC GTA	18
katG WT Amplicon	ATG GCC ATG AAC GAC GTC GAA ACA GCG GCG CTG ATC GTC GGC GGT CAC ACT TTC GGT AAG ACC CAT GGC GCC GGC CCG GCC GAT CTG GTC GGC CCC GAA CCC GAG GCT GCT CCG CTG GAG CAG ATG GGC TTG GGC TGG AAG AGC TCG TAT GGC ACC GGA ACC GGT AAG GAC GCG ATC ACC AGC GGC ATC GAG GTC GTA TGG ACG AAC ACC CCG ACG AAA TGG GAC AAC AGT TTC CTC GAG ATC CTG TAC GGC TAC GAG TGG GAG	264

[a]Nucleotides complementary to the Dza sensor are underlined. Nucleotides complementary to the Dzb sensor are double-underlined. Nucleotides complementary to the target sequence are bolded and underlined. Nucleotides complementary to the substrate are in green. Nucleotides involved in the catalytic core are italicized. Single nucleotide polymorphisms are in red and bolded. Ribonucleotides are in blue and bolded. Sequences corresponding with the fragment of the amplicon are in purple.

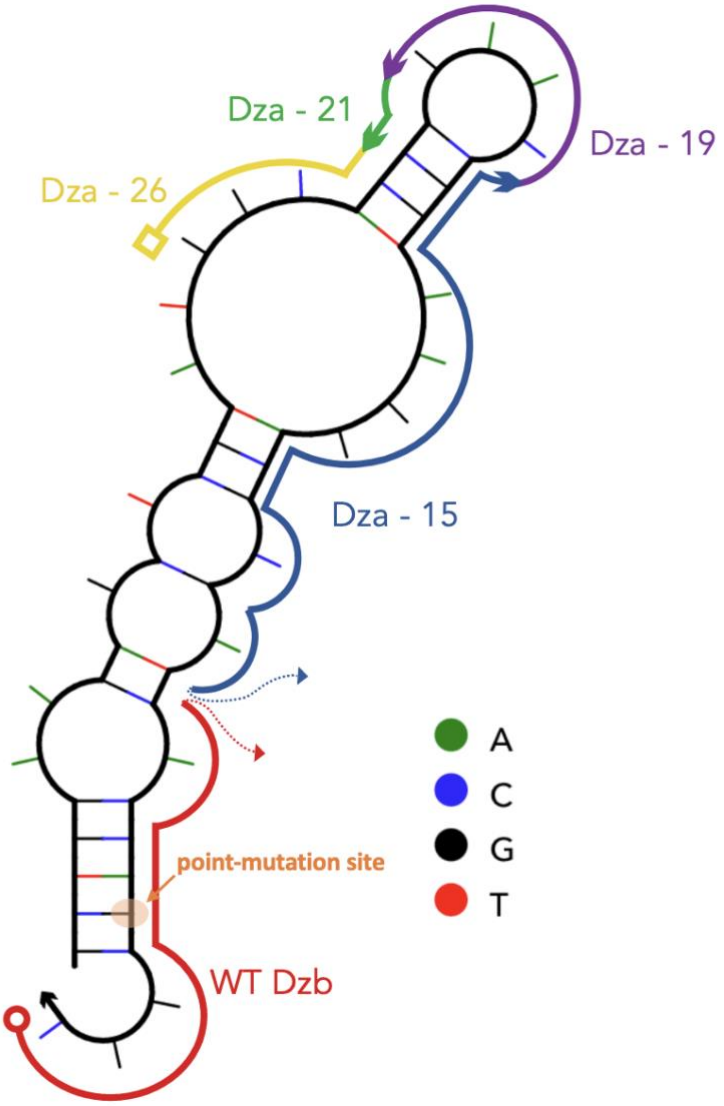

Figure 11: Schematic of synthetic *katG* representing the interrogation by the Dza and Dzb at 54°C and 1uM concentration. The secondary structure of the target was predicted using NUPACK software..[37,38]

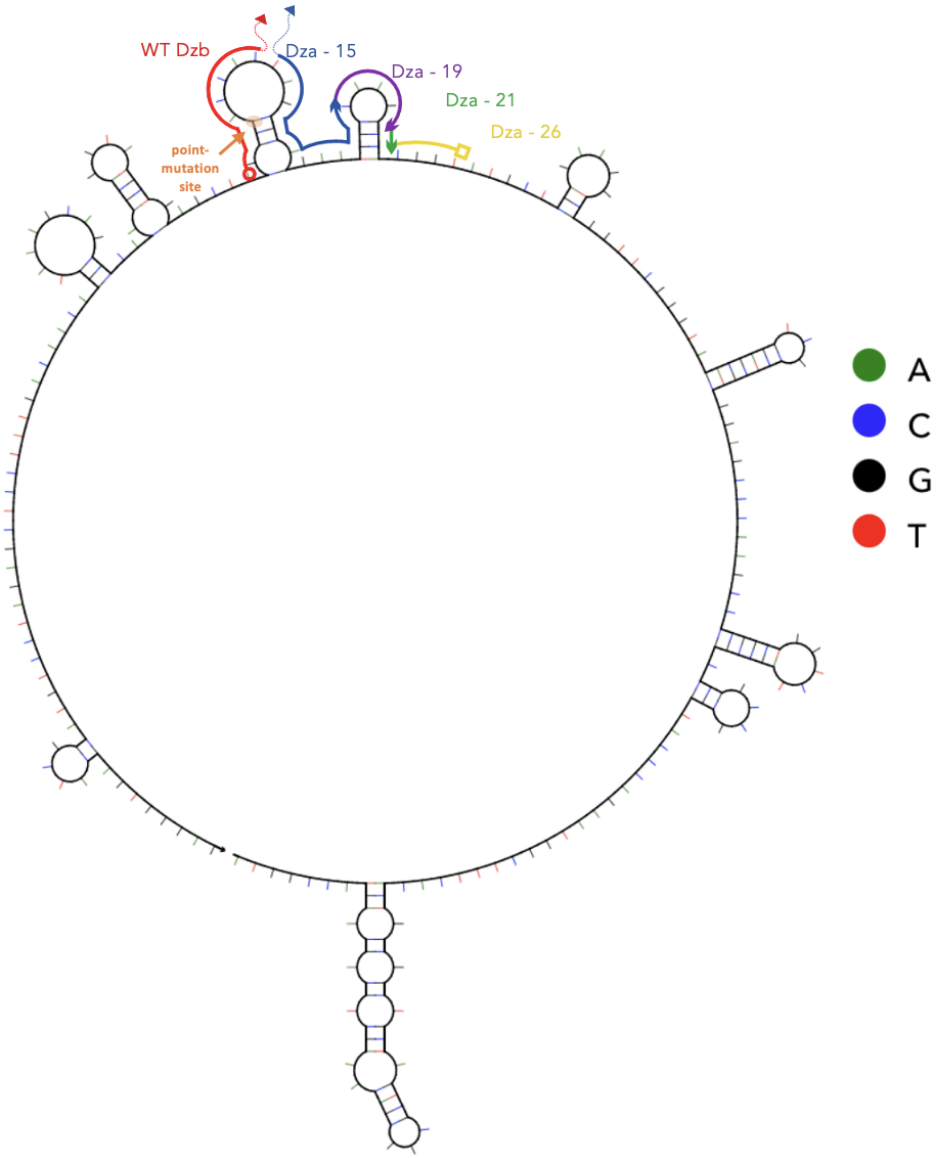

Figure 12: Schematic of *katG* amplicon representing the interrogation by the Dza and Dzb at 54°C and 1uM concentration. The secondary structure of the target was predicted using NUPACK software.[37,38]

It was hypothesized that the elongation of the Dza strand of the sDz probe would increase the affinity of the probe to its complementary target without compromising the discriminating power. The addition of complementary nucleotides to the Dza strand increases the sensor's complementarity to the target, thus increasing catalytic core formation and signal output.

Additionally, Dza sequences in Table 1 were designed to interrogate the synthetic target and *katG* amplicon shown in Figures 10 and 11 at 54 °C, with the intention of increasing the probes response by disrupting secondary structures and stem-loops formed by the target sequence.

3.2 – Optimization of *katG* sensors through nucleotide elongation

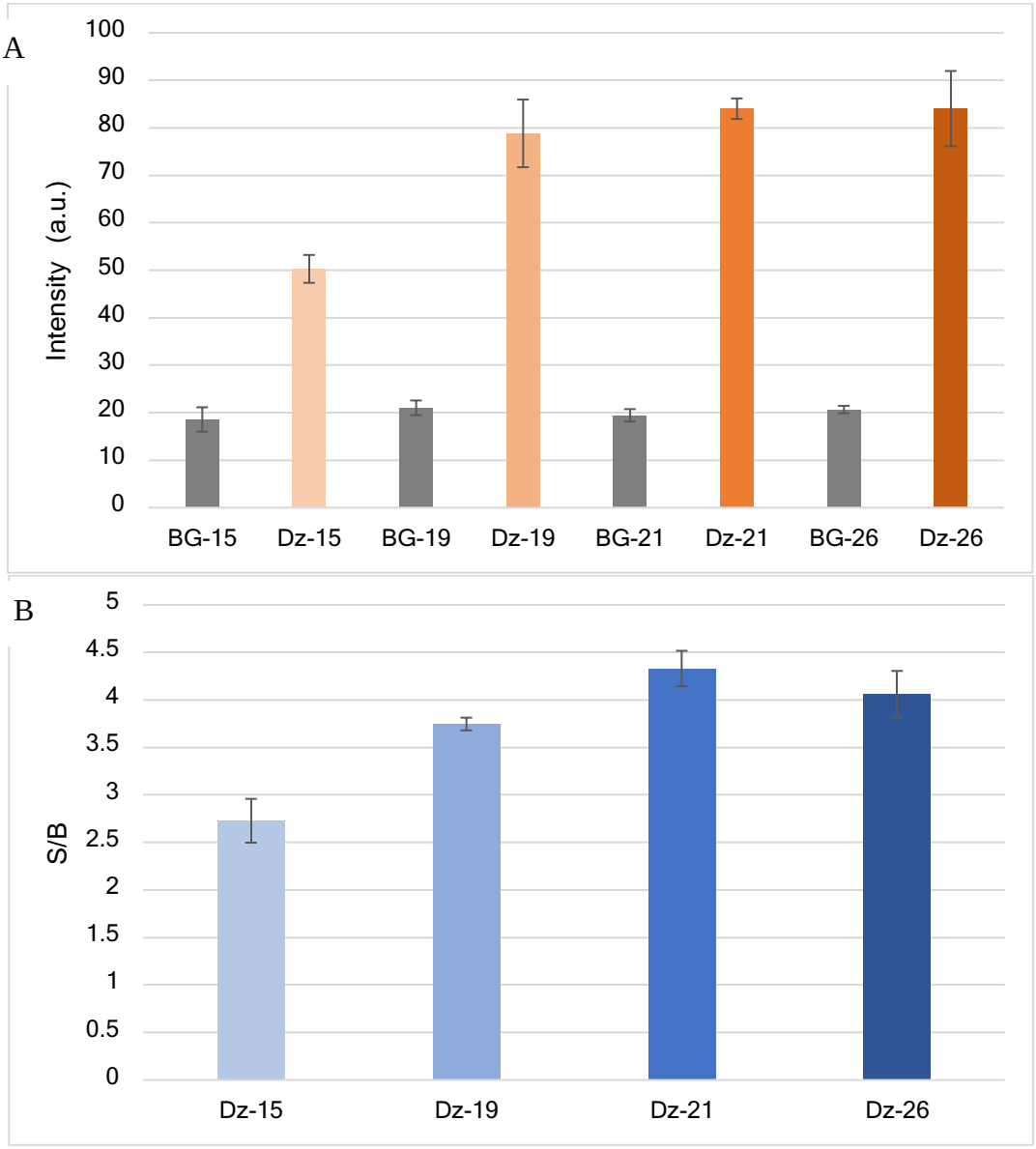

Figure 13: Fluorescent response of the sDz probes interrogating the katG target containing the DzA strand with the indicated length, in nts, of its target-binding arm. A. Raw fluorescence intensity of the samples without the target (BG) or with the WT target (Dz). B. Signal-to-background ratio (S/B) for the indicated sensors was calculated by dividing the target-dependent signal (Dz) by the blank (BG). The data are average valued for 3 independent trials, with standard deviations as error bars.

By increasing the target-binding arm of DzA from 15 to 19 nucleotides, the signal intensity of the probe in the presence of its complementary target increased, as additional nucleotides of DzA-19 would interact with an accessible loop region of the target to provide overall stabilization of the probe-target complex. Additional elongation of DzA did not result in a further increase of the signal, as the signal intensity for the samples containing DzA-19, DzA-21 or Dz-26 were not statistically different (Figure 13A). At the same time, when the background for each of the tested probes was considered to calculate the signal turn-on (S/B), the highest average S/B was observed for Dz-21 (though not statistically different from Dz-26) (Fig. 13B)." It is hypothesized that longer sequence of DzA-26, in comparison with its shorter variants DzA-21, DzA-19 and DzA-15, increases the likelihood of the strand to form partially complementary fragments with DzB, which may result in some catalytical activity of Dz due to association of DzA and DzB in the absence of the target. This would result in higher background.

3.3 – Selectivity analysis of *katG* Dz Sensors

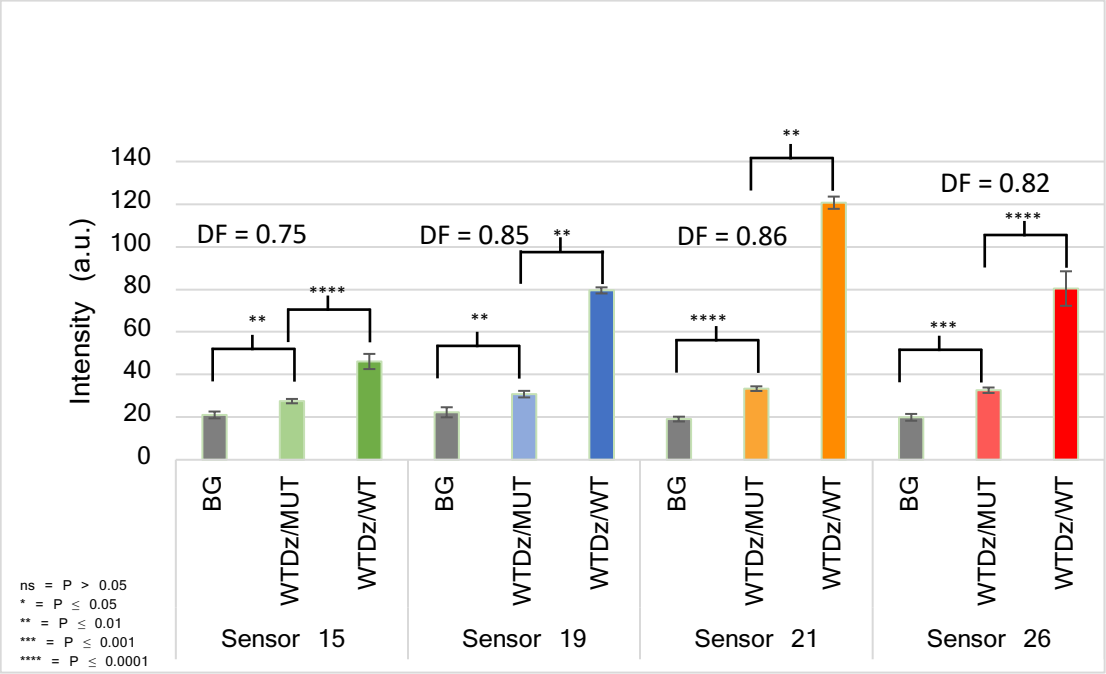

Figure 14: Selectivity analysis via the response of WT Dz sensors with mutant synthetic target compared to the response of WT Dz sensors with WT synthetic target. The data are average valued for 3 independent trials, with standard deviations as error bars.

To explore the selective capabilities of the WT sDz sensors, the sensors were used to interrogate a synthetic target designed to simulate the isoniazid-resistant *katG* sequence (Table 1). Congruent sensor pairs (WTDz and WT target) performed similar to the sensors in Figure 13A, where there is an increase in signal as the sensor lengths increase. Dz-26 shows a decrease in signal, signifying that the sensor at that length has difficulty interrogating the target relative to Dz-21. Statistical analysis was performed via a two-tailed T-test, and it was determined with 95% confidence that the response from the MUT target is statistically different from the WT-triggered response across sensor sets (Figure 14). Non-congruent sensor pairs (WTDz and MUT target) showed a low response regardless of the Dza sensor length. This suggests that the Dzb arm was able to discriminate between the single nucleotide difference in the targets, however,

based on the statistical analysis it was concluded that the sensors are moderately discriminatory. For sDz probes that are very discriminatory, we expect to see signal no statistical difference between the background and the mutant target because there would be no hybridization of the mutant target to the probe. However, the analysis of the response from the WT probe in the presence of the MUT target in comparison with the background revealed a statistically significant difference, signifying there was hybridization of the wildtype sensor in the presence of the mutant target, which facilitates catalytic activity of the core and generates the non-specific signal observed. Additionally, the differentiation factor (DF) was calculated using the following expression:

$$DF = 1 - \left(\frac{MUT - BG}{WT - BG}\right)$$

$$where\ WT = signal\ from\ WT\ target$$

$$MUT = signal\ from\ MUT\ target$$

$$BG = signal\ from\ background.$$

DF was used to determine the similarity between the WT target response and the MUT target response with respect to the background. An ideal DF value is 1, which suggests that the background is indistinguishable from the MUT. Dz-21 displayed the highest DF, 0.86, signifying that the sensor set had the highest discriminatory capabilities to distinguish the presence of the fully complementary target from the mismatched one.

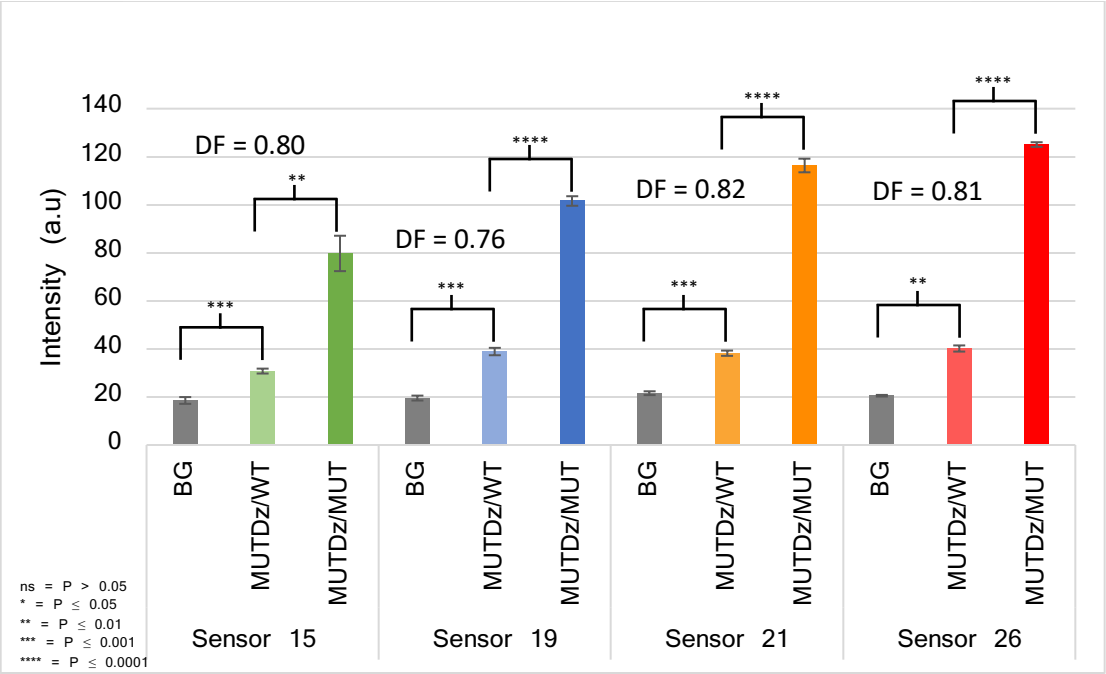

Figure 15: Selectivity analysis via the response of mutant Dz sensors with WT synthetic target compared to the response of WT Dz sensors with WT synthetic target. The data are average valued for 3 independent trials, with standard deviations as error bars.

Alternatively, a set of MUT sensors were used to analyze WT target (Figure 15). The response of the congruent sensor pair (MUT Dz and MUT target) shows an increase in signal as the sensor length is increased and Dz-26 shows the highest intensity. The signal of the background remained consistent at an intensity of 20 a.u. across all sensors. The response of the non-congruent sensor pair (MUT Dz and WT target) remained low, however, there is an increase in signal, particularly between Dz-15 and the rest of the sensors. This can be attributed to the formation of the probe-target complex even in the presence of the mismatch target. It was determined that the responses of the congruent and non-congruent pair are statistically different with 95% confidence. Dz-21 had a DF of 0.82, which showcases that this sensor is the most optimal when analyzing both the wild type and the mutant.

3.4 – Analysis of *katG* amplicon

With the successful response of the Dz sensors with a synthetic target, total BCG DNA was used to amplify the *katG* gene via PCR. Species of *Mycobacterium* share 99% genetic similarities, thus, DNA from *Mycobacterium bovis* BCG, an attenuated culture of *Mycobacterium bovis*, is used as a proxy to complete this study.[39] To determine the effectiveness of the sensors both symmetric and asymmetric PCR methods were employed. It was determined that asymmetric amplification yielded a larger response from sensors than its symmetric counterpart (Figure 17). Successful amplification of the *katG* gene was verified via agarose gel electrophoresis and Figure 15 displays the presence of ssDNA generated from the asymmetric amplification methods. Lane 3 shows two bands at approximately 300 bp, these correlate with the 264 nt *katG* amplicon (Table 1). Based on the principle of asymmetric amplification, dsDNA is generated when both primers are present in the PCR reaction volume. However, due to the unequal primer concentrations, the limiting primer is consumed before the excess primer, thus, yielding ssDNA. Smaller fragments run through the gel at faster rates which explains why 2 bands are observed. The thicker, low-mobility band and the thinner high-mobility band in lane 3 are indicative of dsDNA and ssDNA, respectively. In comparison, the use of equal primer concentration yields a single thick band in lane 5 that has migrated to the same location as the low-mobility band in lane 3. The band in lane 5 is brighter due to the presence of dsDNA product only. The bands in lane 7 share the same appearance as the bands in lane 3 and contain DNA also amplified asymmetrically, but in this case, the RP concentration was greater than that of the FP. It was concluded that ssDNA is most optimal for sDz analysis, and this is depicted in Figure 16 where the Dz-21 was used to probe the amplicons. The fluorescence intensity from the

sDz assay of asymmetrically amplified DNA (FP>RP) is nearly four times the intensity of the background. In the case of symmetric amplification, the sensors showcased difficulty interrogating the amplicon and resulting in a signal comparable to the no template control (NTC). The Dz-21 sensor also had difficulty interrogating the amplicon produced when the RP concentration was greater than the FP, demonstrating a signal equivalent to the NTC. The results of this analysis showed that asymmetric amplification where F>R generates amplicon that could be efficiently interrogated by the sDz probes.

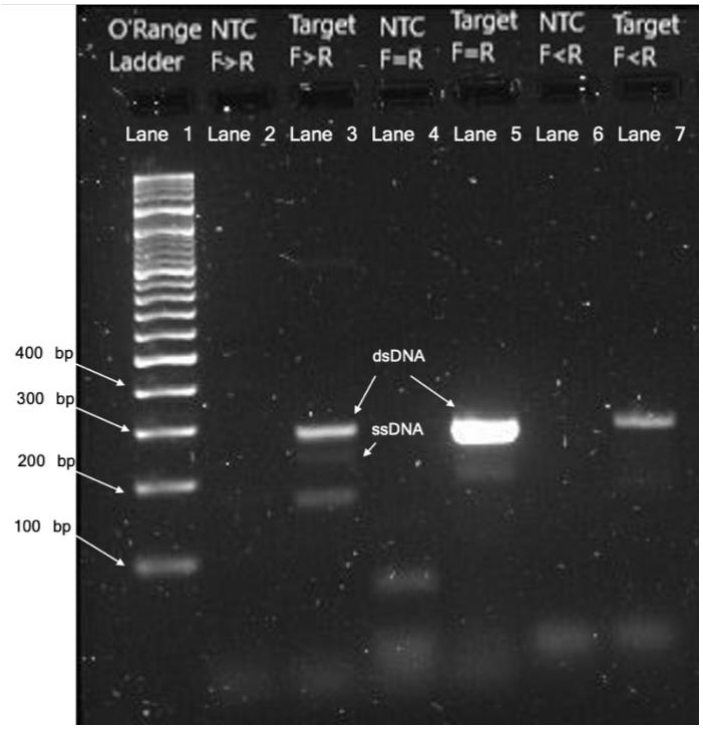

Figure 16: Gel electrophoresis analysis of asymmetric and symmetric PCR of a fragment of the *katG* gene. DNA ladder used is the O'RangeRuler 100 bp DNA Ladder from ThermoFisher.

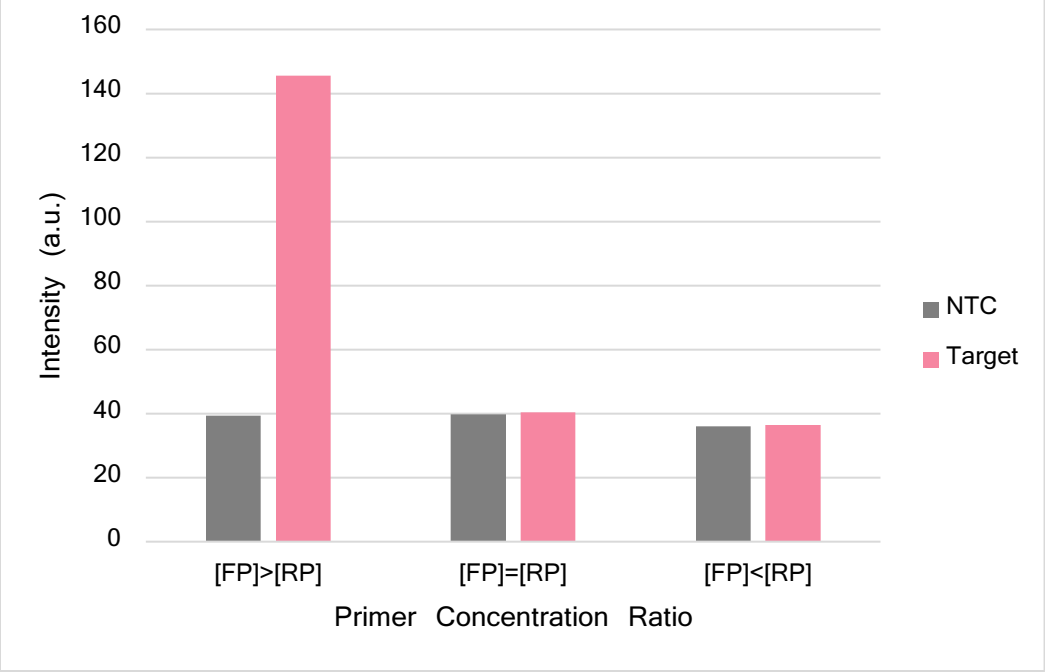

Figure 17: Analysis of *katG* amplicon via asymmetric PCR. The Dz-21 sensor was used to interrogate amplicon generated by asymmetric and symmetric PCR.

Based on the literature the efficiency of asymmetric PCR is poor compared to its symmetric counterpart.[36] They often exhibit low amplification efficiency and require extensive optimization due to the melting temperatures of the unequal primer molar concentrations. LATE-PCR is a suitable alternative where primers are designed to compensate for the concentration differences.[36] To optimize the amplification of the DNA target via LATE-PCR, five primer sets were synthesized by adding nucleotides complementary to the target at the 5' end of the liming primer, the reverse primer in this case (Table 2). It was hypothesized that the implementation of LATE-PCR will generate single-stranded amplicon efficiently, thus, promoting optimization of the sDz assay for Mtb DNA.

Table 2: Oligonucleotide sequences for LATE-PCR analysis of *katG*

Sequence[a]	**Primer Length (nts.)**	**Melting Point**	**ΔT_m**[b]
Excess Primer:	18	64.7°C	-
FP* CTT GGG CTG GAA GAG CTCG			
Limiting Primers:	20	62.5°C	-2
RP1** AGC TCC CAC TCG TAG CCG TA			
RP2** GTC AGC TCC CAC TCG TAG CCG TA	23	65.1°C	+1
RP3** CGT CAG CTC CCA CTC GTA GCC GTA	24	66.9°C	+3
RP4** TTC GTC AGC TCC CAC TCG TAG CCG TA	26	68.1°C	+4
RP5** CTC TTC GTC AGCT CCC ACT CGT AGC CGT A	29	69.2°C	+5

[a]The melting temperatures were predicted using the IDT Oligo Analyzer with the following parameters (IDT, Inc.) using 50 mM Na^+, 1.5 mM Mg^{2+}, 0.2 mM dNTPs and either 0.5 uM (*) or 25 nM (**) primer concentration;

[b]$\Delta T_m = T_m^L - T_m^X$, where T^L and T^X are the melting temperatures for the limiting (reverse in the study) and excess (forward in the study) primer, respectively.

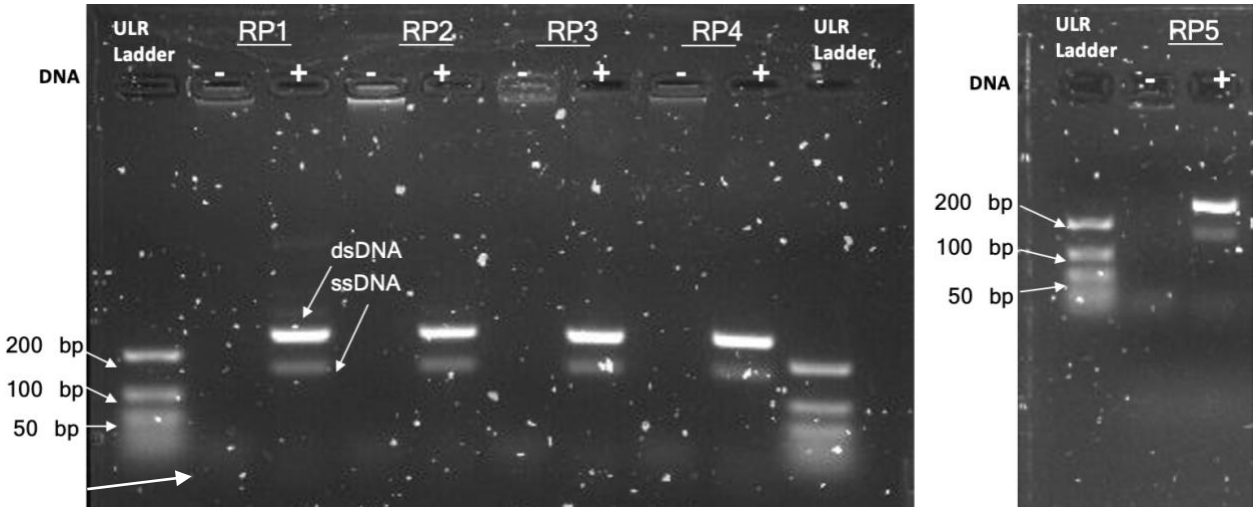

Figure 18: Agarose gel containing *katG* amplicon from LATE-PCR amplification. DNA ladder used is the FastRuler Ultra Low Range (ULR) DNA Ladder from ThermoFisher.

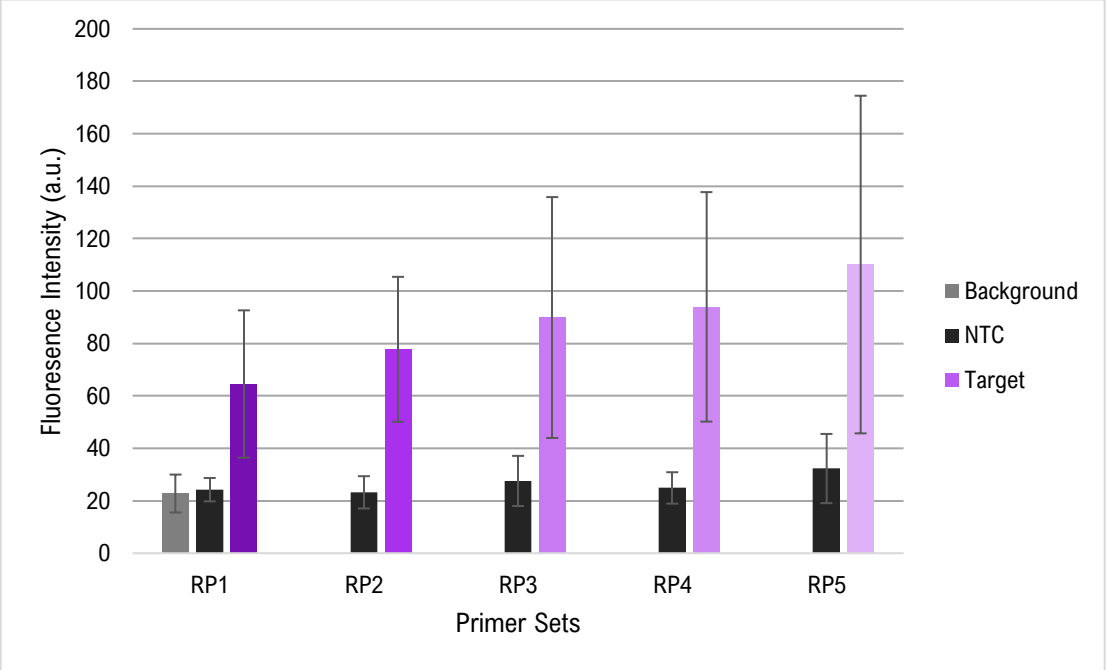

Figure 19: Sensor analysis of *katG* amplicons from LATE-PCR primers. Amplicon was generated via LATE-PCR and interrogated with the Dz-21 sensor set. The data are average valued for 3 independent trials, with standard deviations as error bars.

Based on the literature, primer sets with a $\Delta T_m = T_m^L - T_m^X \geq 0$ should display great amplification efficiency and $\Delta T_m \geq 5$ will have the highest efficiency. [36] Figure 17 depicts that

the *katG* amplicon amplified via LATE-PCR yielded double-stranded and single-stranded products. The band intensity across all primer sets is similar, therefore no conclusions about amplification efficiency can be made from the agarose gel. Figure 18 demonstrates the response to the amplicon after analysis with the Dz-21 sensor set. A trend of increasing fluorescence intensity can be seen as the ΔT_m increases between the primers for LATE-PCR, however, the results were not reproducible. Response of each sensor set was measured in triplicate, however, the intensity of at least one sample was vastly larger than the other two. The efficiency of this amplification method could be improved by increasing the number of PCR cycles. Based on the literature LATE-PCR demonstrates the ability to produce single-stranded product for 70 cycles past the exponential amplification phase.[36]

CHAPTER FOUR: DEOXYRIBOZYME ANALYSIS OF *RPOB*

4.1 – *rpoB* Sensor Design

To interrogate the *rpoB* gene a wildtype (WT) sDz sensor set was designed to target codon 526 (Table 3). SNPs can occur anywhere in the RRDR; however, this study focuses on the interrogation of codon 526. Similar to that of *katG* Dza sensors strands were designed to increase the affinity of the probes which will increase fluorescence response. Dzb sensors strands were synthesized to be discriminatory and probe the point mutation site. The fluorogenic substrate contains the fluorescent dye, Texas Red (TR), which is attached to the 5' end of the sequence. TR is excited at 596 nm, and fluorescence is emitted at 615 nm (λ_{max}). Black Hole Quencher 2 (BHQ2) is attached to the 3' end of the substrate due to its quenching range between 550 and 650 nm. The synthetic target was synthesized based on the sequence of the *rpoB* gene containing codon 526.

Table 3: Oligonucleotide sequences used to analyze *rpoB*

Oligo	**Sequence[a]**	**Length (nts.)**
WT Target	CTG AGC CAA TTC ATG GAC CAG AAC AAC CCG CTG TCG GGG TTG ACC **C**AC AAG CGC CGA CTG TCG GCG CT	68
Mutant Target	CTG AGC CAA TTC ATG GAC CAG AAC AAC CCG CTG TCG GGG TTG ACC **G**AC AAG CGC CGA CTG TCG GCG CT	68
Dza - 17	TAC TTC TCC CAA *GGC TAG CT***C CCG ACA GCG GGT TGT T**	37
Dza - 22	TAC TTC TCC CAA *GGC TAG CT***C CCG ACA GCG GGT TGT TCT GGT**	42
Dza - 30	TAC TTC TCC CAA *GGC TAG CT***C CCG ACA GCG GGT TGT TCT GGT CCA TGA AT**	50

WT Dzb	**CTT GTG GGT CAA C***AC AAC GA*G TGC GCC ATG	30
Fluorogenic substrate	TXR(C6-NH)-CATGGCGCACguTGGGAGAAGTA-(BHQ-2)	23
rpoB FP	GTC GCC GCG ATC AAG GAG TT	20
rpoB RP	CCC TCA GGG GTT TCG ATC GGG	21
WT *rpoB* amplicon	GTC GCC GCG ATC AAG GAG TTC TTC GGC ACC AGC CAG CTG AGC CAA TTC ATG GAC CAG AAC AAC CCG CTG TCG GGG TTG ACC CAC AAG CGC CGA CTG TCG GCG CTG GGG CCC GGC GGT CTG TCA CGT GAG CGT GCC GGG CTG GAG GTC CGC GAC GTG CAC CCG TCG CAC TAC GGC CGG ATG TGC CCG ATC GAA ACC CCT GAG GG	203

[a]Nucleotides complementary to the Dza sensor are underlined. Nucleotides complementary to the Dzb sensor are double-underlined. Nucleotides complementary to the target sequence are bolded and underlined. Nucleotides complementary to the substrate are in green. Nucleotides involved in the catalytic core are italicized. Single nucleotide polymorphisms are in red and bolded. Ribonucleotides are in blue and bolded. Sequences corresponding with the fragment of the amplicon are in purple.

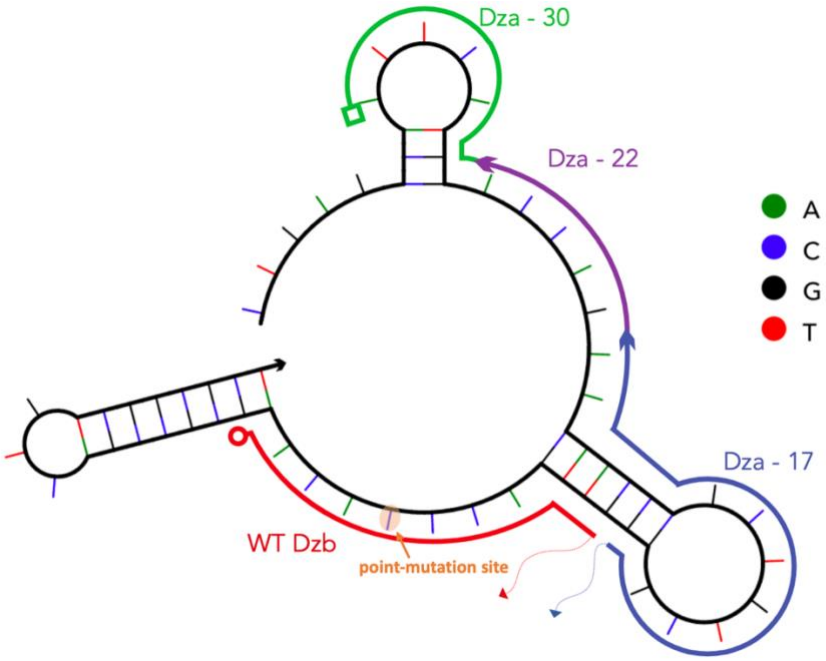

Figure 20: Schematic of synthetic *rpoB* representing the interrogation of the Dza and Dzb at 54°C and 1uM concentration. The secondary structure of the target was predicted using NUPACK software.[37,38]

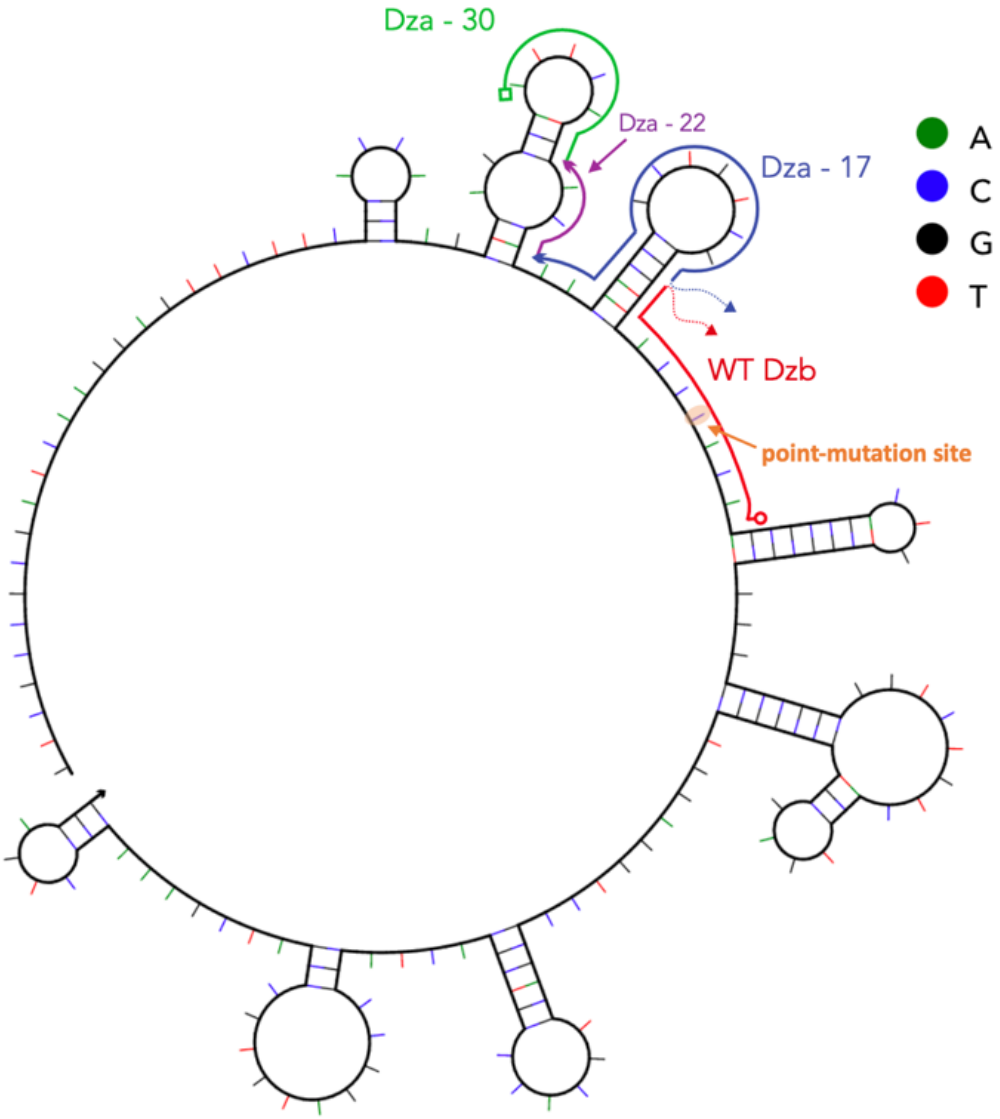

Figure 21: Schematic of *rpoB* amplicon representing the interrogation of the Dza and Dzb at 54°C and 1uM concentration. The secondary structure of the target was predicted using NUPACK software.[37,38]

4.2 – Optimization of *rpoB* sensors through nucleotide elongation

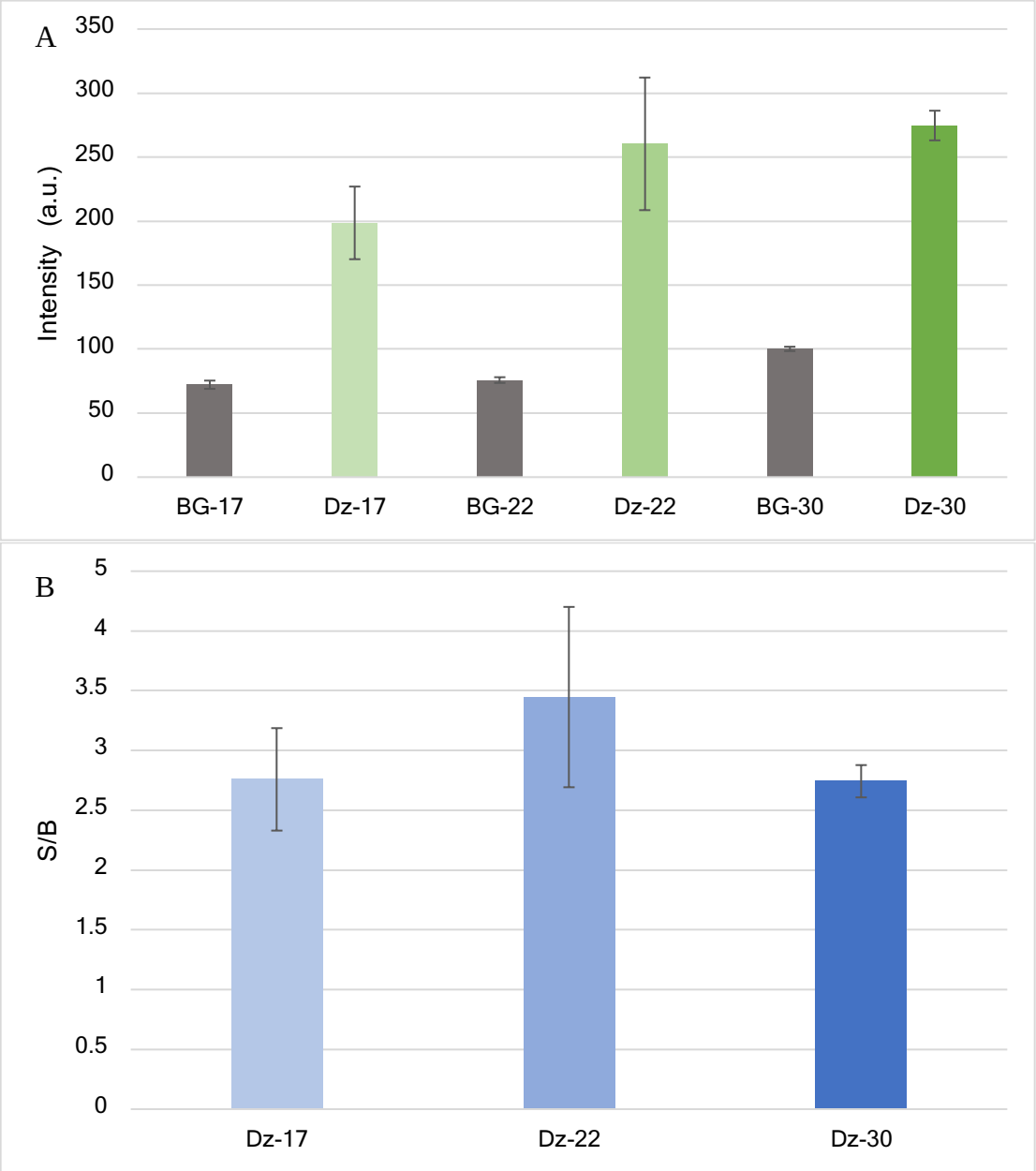

Figure 22: A. Analysis of rpoB gene via signal dependence on sensor length. B. Signal-to-background ratio of elongated rpoB sensors. The data are average valued for 3 independent trials, with standard deviations as error bars.

Extension of the Dza sensor strand resulted in an increase in fluorescence intensity. Dz-30 demonstrates the highest signal intensity among the sensor sets. The background signal

displays an increase as the sensor length increases (Figure 21A). This increase in background signal is predicted to be a result of partial catalytic core formation in the absence of the target. The increase in the background of Dz-30 resulted in a S/B of 2.7 which represents successful interrogation of the sensors (Figure 21B).

4.3 - Selectivity analysis of *rpoB* Dz Sensors

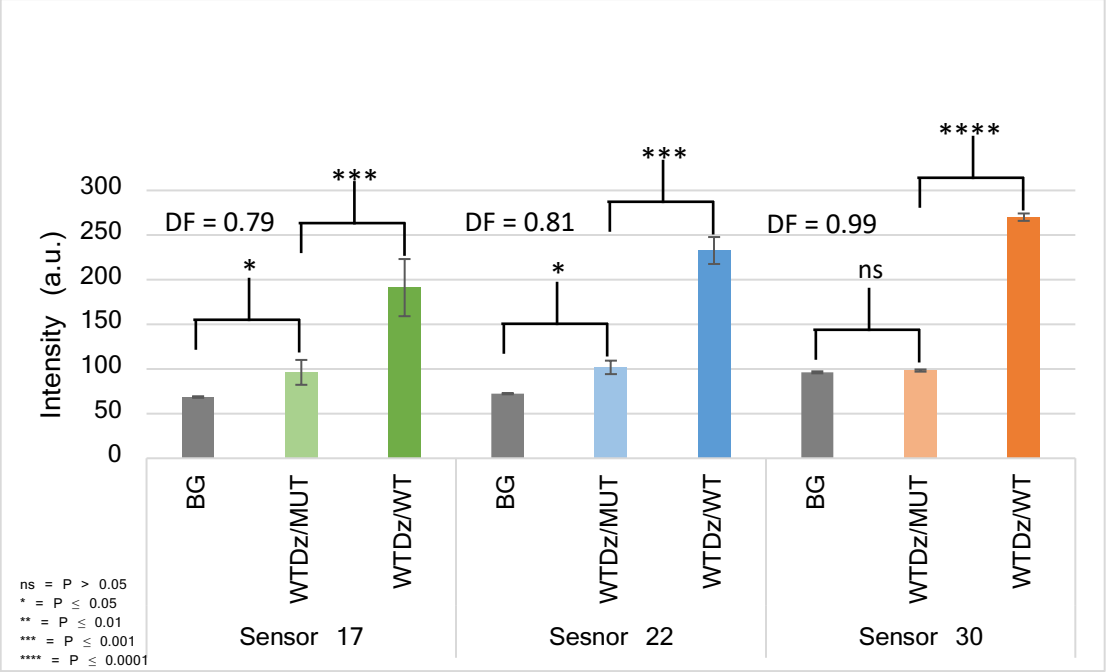

Figure 23: Selectivity analysis via the response of WT Dz sensors with mutant synthetic target compared to the response of WT Dz sensors with WT synthetic target. The data are average valued for 3 independent trials, with standard deviations as error bars.

The efficacy of the sDz to interrogate the mutant target was analyzed using the Dzb sensor designed for the rifampin-susceptible *rpoB* sequence (Table 3). Congruent sensor pairs displayed the same trend seen in Figure 22A, where the fluorescence intensity increased as the sensor length increased. Across all non-congruent sensor pairs an intensity of about 100 a.u was observed. The Dzb arm was able to remain selective in the presence of mutant target. Statistical

analysis was performed, and it was determined with 95% confidence that the response from the MUT target is significantly statistically different from that of the WT target across all sDz. Also, sensor sets showed discriminatory capabilities towards the SNP and Dz-30 displayed the highest DF of 0.99. Due to the DF, Dz-30 was selected as the most optimal sensor, however, Dz-22 was used in some experiments due to its high S/B (Figure 21B)

4.4 – Analysis of *rpoB* Amplicon

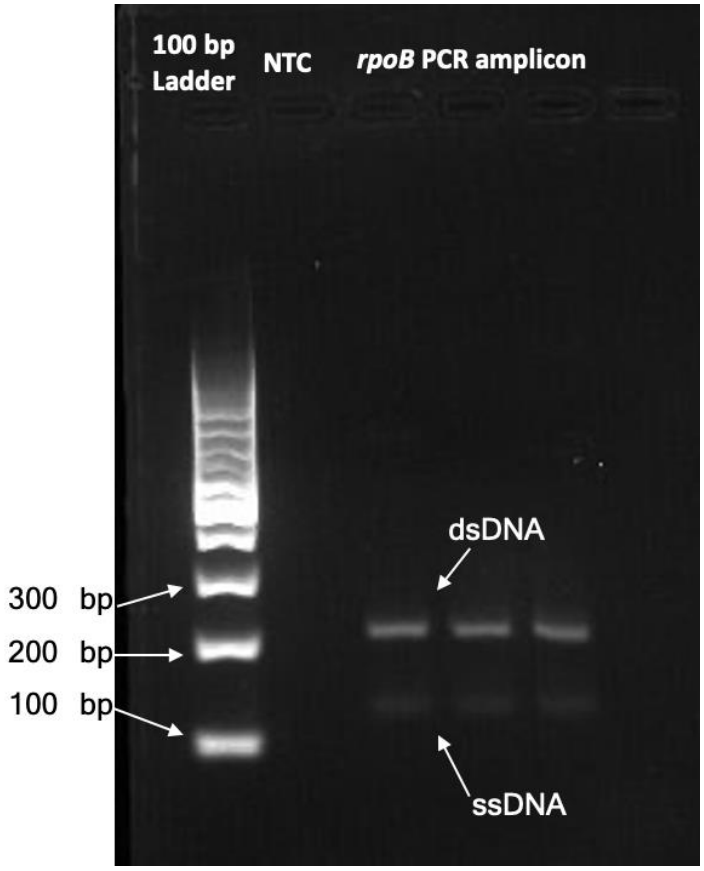

Figure 24: Agarose gel containing rpoB amplicon via traditional aPCR. Bands in lanes 3, 4, and 5 are rpoB amplicon generated under identical conditions.

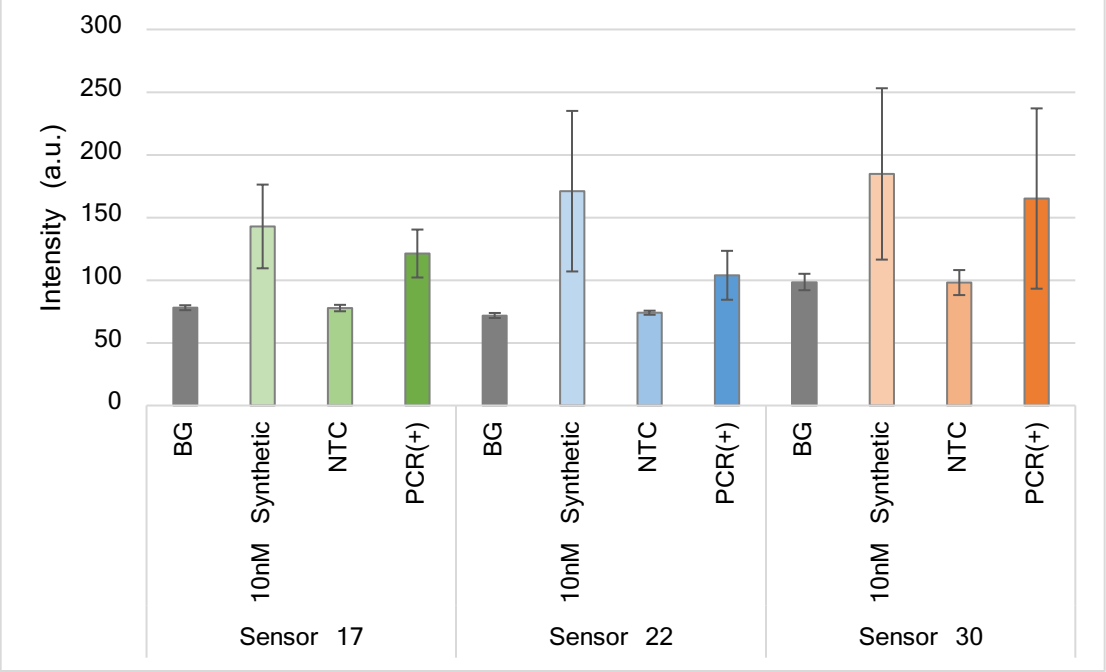

Figure 25: Performance of the rpoB-specific sDz probes (sensors) containing the DzA strands of different lengths. BG is the background signal (in the absence of any target); NTC - PCR no-target control; PCR(+) - PCR amplicon generated by a traditional aPCR using total mycobacterial DNA as a template; Synthetic - the sample in the presence of synthetic WT target corresponding to the amplified sequence of the rpoB gene. The data is an average from 6 independent experiments, with error bars in the form of standard deviations.

Traditional aPCR was performed on Mtb DNA to yield single-stranded *rpoB* amplicon (Figure 23). Figure 24 displays the response of the amplicon across all sensor sets. Due to the large amounts of error, there is no identifiable trend across the 3 sensors. To better optimize the sDz assay, amplification via LATE PCR was used to improve amplification efficiency.

Table 4: Oligonucleotide sequences for LATE-PCR analysis of *rpoB*

Sequence[a]	**Primer Length (nts.)**	**Melting Point**	**ΔT_m**
Excess Primer:	18	64.7°C	-
FP* CTT GGG CTG GAA GAG CTCG			
Limiting Primers:	23	63.1°C	2.9°C
RP1** GCC CCT CAG GGG TTT CGA TCG GG			
RP2** GGG CCC CTC AGG GGT TTC GAT CGG G	25	66.3°C	6.1°C
RP3** GTT GGG CCC CTC AGG GGT TTC GAT CGG G	28	66.9°C	6.7°C

[a]The melting temperatures were predicted using the IDT Oligo Analyzer with the following parameters (IDT, Inc.) using 50 mM Na^+, 1.5 mM Mg^{2+}, 0.2 mM dNTPs and either 0.5 uM (*) or 25 nM (**) primer concentration;

[b]$\Delta T_m = T_m^L - T_m^X$, where T^L and T^X are the melting temperatures for the limiting (reverse in the study) and excess (forward in the study) primer, respectively.

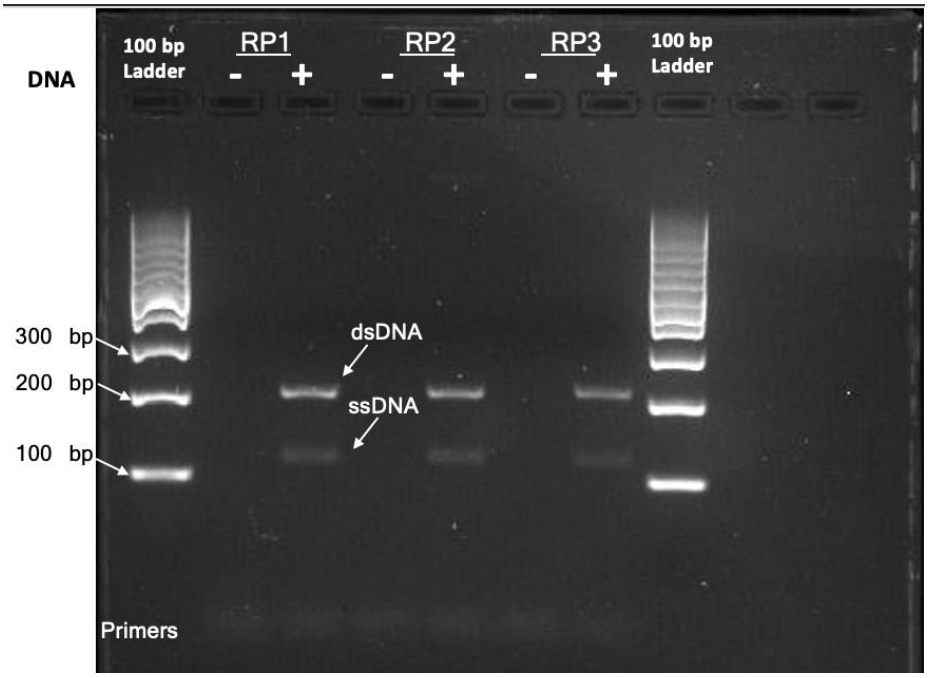

Figure 26: Agarose gel electrophoresis analysis of the *rpoB* amplicons generated via LATE-PCR using the indicated limiting primer.

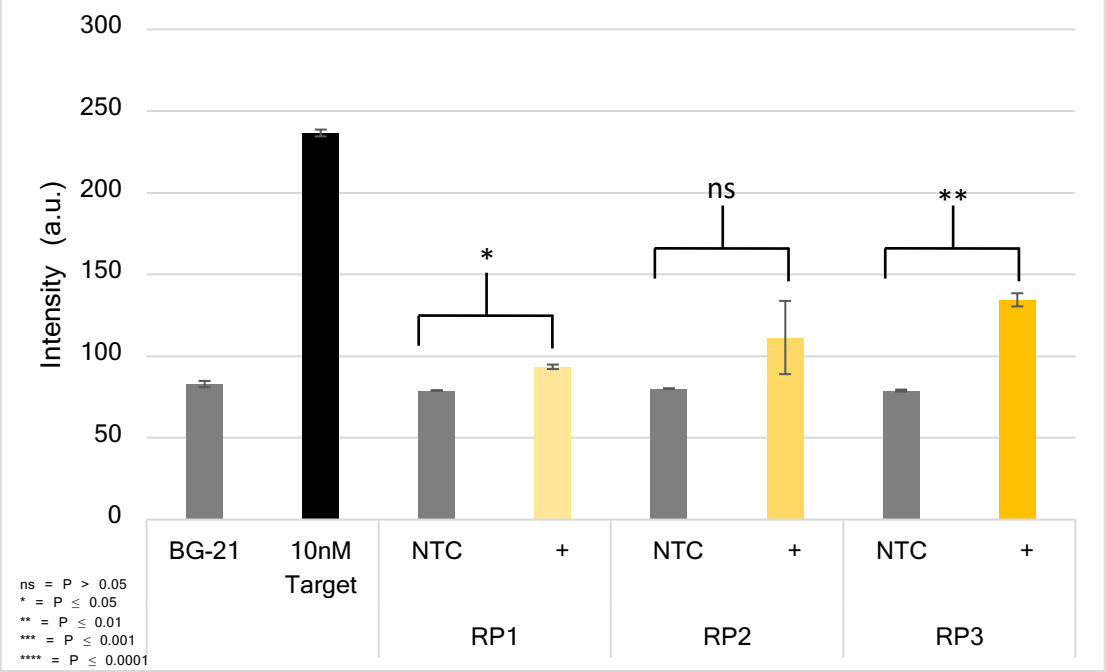

Figure 27: Analysis of the rpoB amplicon generated via LATE-PCR by a fluorescent assay using the Dz-22 probe. The limiting primers used are indicated. NTC - PCR no-target control. BG-21 - background measured for the sample in the absence of any target. As a positive control, 10 nM synthetic WT target was used. The data is an average of 2 independent experiments, with error bars as standard deviations.

LATE-PCR primer sets were designed such that $\Delta T_m \geq 0$ °C. Three primer sets were used - FP/RP1, FP/RP2, and FP/RP3 - with ΔT_m values of 2.9 °C, 6.1 °C, and 6.7 °C, respectively (Table 4). *rpoB* amplicon successfully was generated via LATE-PCR, the low-mobility band near the 200 bp marker is indicative of the 204 nt *rpoB* gene fragment. The bright low-mobility band contains dsDNA and the faint high-mobility band contains ssDNA. Even though the amplicons' band intensities upon gel electrophoresis analysis were comparable for all primers used (Figure 26), the primer sets FP/RP1 and FP/RP3 resulted in the amplicon that triggered a signal with Dz-22 that was statistically different from the signal in the presence of the PCR NTC (Figure 27). However, the data displays an increase in signal output as the ΔT_m increases. This suggests that a higher amount of single-stranded amplicon is being generated as the ΔT_m

increases. With higher amplification efficiency, the more single-stranded amplicon is generated and can be successfully interrogated by sDz. Amplicon generated from RP3 showcased the highest signal among the primer sets. This observation correlates with the conclusion in the paper by Pierce et al. that $\Delta T_m \geq 5°C$ will yield the most efficient amplification.[36] This interrogation can be further optimized by synthesizing another set of primers where $\Delta T_m \geq 7°C$ or increasing the number of PCR cycles.

CHAPTER FIVE: DISCUSSION

In this study, we sought to develop and optimize a deoxyribozyme assay to supplement drug susceptibility testing by increasing the options for molecular analysis of the *katG* and *rpoB* genes from *Mycobacterium tuberculosis* complex. The two main goals of this study were to optimize sensors to increase signal in the presence of the target sequence and optimize asymmetric amplification techniques of Mtb DNA.

In Chapter 3, we aimed to explore the capabilities of sDz sensors with *katG* target. The elongation of the target-binding arm of the universal strand of sDz probe helped to improve target interrogation, resulting in increased signal output. sDz probes designed to recognize either wild-type or mutant *katG* sequences reliably discriminated between the target sequences, however, the signal triggered by the non-congruent target was higher than the background requires further optimization. The sensor set with the 21-nucleotide target binding arm in the universal strand exhibited the most optimal performance, while selectivity remains to be optimized to ensure the non-specific signal at the background level. Selectivity can be improved by shortening the target-binding arm of the Dzb sensor. Editing the sensor in this way may inhibit the formation of the catalytic core in the absence of the target. Another method for improving selectivity is by creating a conformational constraint in the form of a stem-loop in the target binding arm of the Dzb sensor strand. The addition of a stem-loop lowers the free energy of the probe in the dissociated state (where the Dzb sensor strand is not hybridized to the target), and the secondary structure is stabilized by entropy which prevents hybridization of the Dzb sensor to the target. Upon heating, the free energy is increased, and entropy is decreased; this destabilizes the stem-loop and encourages the parts of the probe to enter the associated state

(where the Dzb sensor strand is hybridized to target). In the associated state, a complementary match will have a lower free energy than that of the dissociated state, pushing the reaction in the forward direction where Dzb is bound to the target. Contrarily, in the presence of a mismatch, the free energy will be higher than that of the dissociated state, pushing the reaction in the reverse direction to the dissociated state.[40]

Amplifying the target asymmetrically produced ssDNA amplicon that allows more efficient interrogation by sensors, employing the LATE PCR method shows promise in enhancing the sDz assay by promoting efficient amplification to generate more single-stranded product. In future work, the efficiency of LATE PCR can be improved by increasing the number of cycles and adjusting annealing temperatures and primer concentration ratios.

In Chapter 4, we sought to optimize the response of sDz designed to probe the 526 codon of the *rpoB* gene. Through the elongation of the target-binding region of the Dza strand proved to increase signal input and all sDz sensor sets were able to reliably differentiate between the wildtype and the mutant target sequences. The probe containing the 30-nucleotide target-binding arm in the universal strand proved to be the most selective one with a differentiation factor of 0.99. LATE-PCR yielded a single-stranded product that could be analyzed using the sDz probe and the use of RP3 for LATE-PCR resulted in the amplicon that triggered a signal of the sDz probe that was statistically different from that of the no-target control. Response from the sensors can be increased by increasing the number of PCR cycles, which will generate more single-stranded amplicon. [36]

CHAPTER SIX: CONCLUSIONS

The success of the sensor optimization can be used in future work for assay development. Sensors can be used in the 2-step multiplex capacity where both *katG* and *rpoB* genes are amplified in a single tube via LATE-PCR. Following amplification, the amplicon can be analyzed by both probes at the same time. Based on preliminary studies conducted in our lab, *katG*, and *rpoB* sensors can be read using the portable Quantus fluorometer. This instrument can read fluorescence in a red and blue channel, which corresponds with the fluorophores Texas Red and FAM, respectively. Similar multicomponent deoxyribozyme sensors were previously used for a one-tube assay in a quantitative PCR (qPCR) format, where Mtb DNA is amplified using qPCR and interrogated by Dz in real time all in the same tube.[41] Real-time detection requires phosphorylation to the 3' end of sDz sensors to prevent the extension of sensor sequences by the DNA polymerase during qPCR. In addition, as the activity of the 10-23 catalytic core used in the sDz assay requires a certain concentration of divalent ions (e.g. Mg^{2+}), and the enzyme used in qPCR is inhibited at too high magnesium concentration, optimization of the buffer used for the one-tube PCR/sDz assay is required for the efficient signal generation.[27,42] Finally, regardless of the format, characterization of the assay in terms of limit of detection (LOD) and/or limit of quantification (LOQ) is required, as well as validation of the method under development using clinical samples.

In a clinical setting, wild-type-specific probes and mutant-specific probes can be used together to make conclusive statements about TB infection. Testing a sample with the wild-type specific sensor and receiving a low response will suggest that a patient either doesn't have TB or they have a drug-resistant form of TB. When followed up with the use of mutant-specific

sensors, infection from drug-resistant TB can be confirmed. This series of testing can also reveal cases of antimicrobial heteroresistance. In this respect, additional characterization of the ability of the probes to detect drug-resistant bacterial populations in excess of drug-susceptible bacterial strains.

While displaying great biosensor capabilities, our sensors still have some limitations. The use of the sDz fails to detect mutations outside of codons 315 (*katG*) and 526 (*rpoB*). This is particularly unfortunate when detecting RIF resistance because resistance is conferred through point mutations (SNPs and deletions) at other codons in the 81-base pair RDRR.[17] To interrogate different SNPs in other codons, the implementation of multiple probes for each region is necessary. Another drawback of the PCR/sDz probe approach reported here is the requirement for bacterial DNA to be isolated from clinical samples. The WHO-endorsed technology for TB detection and molecular DST , Xpert MTB/XDR, includes capabilities for sample processing, bacterial lysis, and DNA capturing, therefore, for its application in practice, the PCR/sDz assay needs to be combined with a device that enables processing of the clinical samples and a DNA purification step.[8] Lastly, sDz sensors would still require bacteriological confirmation by a method approved by the WHO and would act as a supplement diagnostic method to DST. Despite the drawbacks, sDz technology shows great promise in detecting mutant Mtb strains and is a cost-effective, user-friendly assay that can advance molecular diagnostic techniques in Mtb-riddled areas where resources are scarce.

LIST OF REFERENCES

(1) Global Tuberculosis Report 2022. Geneva: World Health Organization; 2022.

(2) Centers for Disease Control and Prevention, Division of Tuberculosis Elimination, National Center for HIV, Viral Hepatitis, STD, and TB Prevention, Last Revised February 2023. Https://Www.Cdc.Gov/Tb/Topic/Basics/Signsandsymptoms.Htm#print (Accessed 2023-02-25).

(3) Allué-Guardia, A.; García, J. I.; Torrelles, J. B. Evolution of Drug-Resistant Mycobacterium Tuberculosis Strains and Their Adaptation to the Human Lung Environment. *Front. Microbiol.* **2021**, *12*. https://doi.org/10.3389/fmicb.2021.612675.

(4) Rufai, S. B.; Kumar, P.; Singh, A.; Prajapati, S.; Balooni, V.; Singh, S. Comparison of Xpert MTB/RIF with Line Probe Assay for Detection of Rifampin-Monoresistant Mycobacterium Tuberculosis. *J. Clin. Microbiol.* **2014**, *52* (6), 1846–1852. https://doi.org/10.1128/JCM.03005-13.

(5) Seung, K. J.; Keshavjee, S.; Rich, M. L. Multidrug-Resistant Tuberculosis and Extensively Drug-Resistant Tuberculosis. *Cold Spring Harb. Perspect. Med.* **2015**, *5* (9), a017863. https://doi.org/10.1101/cshperspect.a017863.

(6) Siddiqi, S.; Ahmed, A.; Asif, S.; Behera, D.; Javaid, M.; Jani, J.; Jyoti, A.; Mahatre, R.; Mahto, D.; Richter, E.; Rodrigues, C.; Visalakshi, P.; Rüsch-Gerdes, S. Direct Drug Susceptibility Testing of Mycobacterium Tuberculosis for Rapid Detection of Multidrug Resistance Using the Bactec MGIT 960 System: A Multicenter Study. *J. Clin. Microbiol.* **2012**, *50* (2), 435–440. https://doi.org/10.1128/JCM.05188-11.

(7) Line Probe Assays for Detection of Drug-Resistant Tuberculosis: Interpretation and Reporting Manual for Laboratory Staff and Clinicians. Geneva: World Health Organization; 2022. Licence: CC BY-NC-SA 3.0 IGO.

(8) Lawn, S. D.; Nicol, M. P. Xpert® MTB/RIF Assay: Development, Evaluation and Implementation of a New Rapid Molecular Diagnostic for Tuberculosis and Rifampicin Resistance. *Future Microbiol.* **2011**, *6* (9), 1067–1082. https://doi.org/10.2217/fmb.11.84.

(9) Goel, G.; Kumar, A.; Puniya, A. K.; Chen, W.; Singh, K. Molecular Beacon: A Multitask Probe. *J. Appl. Microbiol.* **2005**, *99* (3), 435–442. https://doi.org/10.1111/j.1365-2672.2005.02663.x.

(10) Cornett, E. M.; Campbell, E. A.; Gulenay, G.; Peterson, E.; Bhaskar, N.; Kolpashchikov, D. M. Molecular Logic Gates for DNA Analysis: Detection of Rifampin Resistance in M. Tuberculosis DNA. *Angew. Chem. Int. Ed Engl.* **2012**, *51* (36), 9075–9077. https://doi.org/10.1002/anie.201203708.

(11) Purkan, P.; Ihsanawati, I.; Natalia, D.; Syah, Y. M.; Retnoningrum, D. S.; Siswanto, I. Molecular Analysis of KatG Encoding Catalase-Peroxidase from Clinical Isolate of Isoniazid-Resistant Mycobacterium Tuberculosis. *J. Med. Life* **2018**, *11* (2), 160–167.

(12) Palomino, J. C.; Martin, A. Drug Resistance Mechanisms in Mycobacterium Tuberculosis. *Antibiot. Basel Switz.* **2014**, *3* (3), 317–340. https://doi.org/10.3390/antibiotics3030317.

(13) Vilchèze, C.; Jacobs, W. R. J. Resistance to Isoniazid and Ethionamide in Mycobacterium Tuberculosis: Genes, Mutations, and Causalities. *Microbiol. Spectr.* **2014**, *2* (4), MGM2-0014–2013. https://doi.org/10.1128/microbiolspec.MGM2-0014-2013.

(14) Lempens, P.; Meehan, C. J.; Vandelannoote, K.; Fissette, K.; de Rijk, P.; Van Deun, A.; Rigouts, L.; de Jong, B. C. Isoniazid Resistance Levels of Mycobacterium Tuberculosis Can Largely Be Predicted by High-Confidence Resistance-Conferring Mutations. *Sci. Rep.* **2018**, *8* (1), 3246. https://doi.org/10.1038/s41598-018-21378-x.

(15) Hazbón, M. H.; Brimacombe, M.; Bobadilla del Valle, M.; Cavatore, M.; Guerrero, M. I.; Varma-Basil, M.; Billman-Jacobe, H.; Lavender, C.; Fyfe, J.; García-García, L.; León, C. I.; Bose, M.; Chaves, F.; Murray, M.; Eisenach, K. D.; Sifuentes-Osornio, J.; Cave, M. D.; Ponce de León, A.; Alland, D. Population Genetics Study of Isoniazid Resistance Mutations and Evolution of Multidrug-Resistant Mycobacterium Tuberculosis. *Antimicrob. Agents Chemother.* **2006**, *50* (8), 2640–2649. https://doi.org/10.1128/AAC.00112-06.

(16) Napier, G.; Campino, S.; Phelan, J. E.; Clark, T. G. Large-Scale Genomic Analysis of Mycobacterium Tuberculosis Reveals Extent of Target and Compensatory Mutations Linked to Multi-Drug Resistant Tuberculosis. *Sci. Rep.* **2023**, *13* (1), 623. https://doi.org/10.1038/s41598-023-27516-4.

(17) Miller L P; Crawford J T; Shinnick T M. The RpoB Gene of Mycobacterium Tuberculosis. *Antimicrob. Agents Chemother.* **1994**, *38* (4), 805–811. https://doi.org/10.1128/AAC.38.4.805.

(18) Yue, J.; Shi, W.; Xie, J.; Li, Y.; Zeng, E.; Wang, H. Mutations in the RpoB Gene of Multidrug-Resistant Mycobacterium Tuberculosis Isolates from China. *J. Clin. Microbiol.* **2003**, *41* (5), 2209–2212. https://doi.org/10.1128/JCM.41.5.2209-2212.2003.

(19) Chen, Y.-X.; Javid, B. More than Merely Drug Resistance. *Nat. Microbiol.* **2018**, *3* (10), 1078–1079. https://doi.org/10.1038/s41564-018-0250-3.

(20) McManus, S. A.; Li, Y. The Structural Diversity of Deoxyribozymes. *Mol. Basel Switz.* **2010**, *15* (9), 6269–6284. https://doi.org/10.3390/molecules15096269.

(21) Silverman, S. K. Catalytic DNA: Scope, Applications, and Biochemistry of Deoxyribozymes. *Trends Biochem. Sci.* **2016**, *41* (7), 595–609. https://doi.org/10.1016/j.tibs.2016.04.010.

(22) Gerasimova, Y. V.; Kolpashchikov, D. M. Nucleic Acid Detection Using MNAzymes. *Chem. Biol.* **2010**, *17* (2), 104–106. https://doi.org/10.1016/j.chembiol.2010.02.003.

(23) Santoro, S. W.; Joyce, G. F. A General Purpose RNA-Cleaving DNA Enzyme. *Proc. Natl. Acad. Sci. U. S. A.* **1997**, *94* (9), 4262–4266. https://doi.org/10.1073/pnas.94.9.4262.

(24) Wong, B. C.; Abu Bakar, J.; Dhanoa, A.; Tan, H. S. RNA-Cleaving DNAzymes as a Diagnostic and Therapeutic Agent against Antimicrobial Resistant Bacteria. *Curr. Genet.* **2022**, *68* (1), 27–38. https://doi.org/10.1007/s00294-021-01212-0.

(25) Rosenbach, H.; Victor, J.; Etzkorn, M.; Steger, G.; Riesner, D.; Span, I. Molecular Features and Metal Ions That Influence 10-23 DNAzyme Activity. Molecules 2020, 25, 3100. Https://Doi.Org/10.3390/Molecules25133100.

(26) Cairns, M. J.; King, A.; Sun, L. Optimisation of the 10–23 DNAzyme–Substrate Pairing Interactions Enhanced RNA Cleavage Activity at Purine–Cytosine Target Sites. *Nucleic Acids Res.* **2003**, *31* (11), 2883–2889. https://doi.org/10.1093/nar/gkg378.

(27) Grimpe, B. Deoxyribozymes: New Therapeutics to Treat Central Nervous System Disorders. *Front. Mol. Neurosci.* **2011**, *4*, 25. https://doi.org/10.3389/fnmol.2011.00025.

(28) Santoro, S. W.; Joyce, G. F. Mechanism and Utility of an RNA-Cleaving DNA Enzyme. *Biochemistry* **1998**, *37* (38), 13330–13342. https://doi.org/10.1021/bi9812221.

(29) Mokany, E.; Bone, S. M.; Young, P. E.; Doan, T. B.; Todd, A. V. MNAzymes, a Versatile New Class of Nucleic Acid Enzymes That Can Function as Biosensors and Molecular Switches. *J. Am. Chem. Soc.* **2010**, *132* (3), 1051–1059. https://doi.org/10.1021/ja9076777.

(30) The Polymerase Chain Reaction: An Overview and Development of Diagnostic PCR Protocols at the LCDC. *Can. J. Infect. Dis. J. Can. Mal. Infect.* **1991**, *2* (2), 89–91. https://doi.org/10.1155/1991/580478.

(31) Abramson, R. D. Thermostable DNA Polymerases. In *PCR Strategies*; Innis, M. A., Gelfand, D. H., Sninsky, J. J., Eds.; Academic Press: San Diego, 1995; pp 39–57. https://doi.org/10.1016/B978-012372182-2/50006-X.

(32) Kralik, P.; Ricchi, M. A Basic Guide to Real Time PCR in Microbial Diagnostics: Definitions, Parameters, and Everything. *Front. Microbiol.* **2017**, *8*, 108. https://doi.org/10.3389/fmicb.2017.00108.

(33) Britannica, The Editors of Encyclopaedia. "Polymerase Chain Reaction". Encyclopedia Britannica, 6 Jan. 2023, Https://Www.Britannica.Com/Science/Polymerase-Chain-Reaction. Accessed 27 March 2023.

(34) Nehdi, A.; Samman, N.; Aguilar-Sánchez, V.; Farah, A.; Yurdusev, E.; Boudjelal, M.; Perreault, J. Novel Strategies to Optimize the Amplification of Single-Stranded DNA. *Front. Bioeng. Biotechnol.* **2020**, *8*, 401. https://doi.org/10.3389/fbioe.2020.00401.

(35) Rychlik, W.; Spencer, W. J.; Rhoads, R. E. Optimization of the Annealing Temperature for DNA Amplification in Vitro. *Nucleic Acids Res.* **1990**, *18* (21), 6409–6412. https://doi.org/10.1093/nar/18.21.6409.

(36) Pierce, K. E.; Sanchez, J. A.; Rice, J. E.; Wangh, L. J. Linear-After-The-Exponential (LATE)-PCR: Primer Design Criteria for High Yields of Specific Single-Stranded DNA and Improved Real-Time Detection. *Proc. Natl. Acad. Sci. U. S. A.* **2005**, *102* (24), 8609–8614. https://doi.org/10.1073/pnas.0501946102.

(37) Fornace, M. E.; Porubsky, N. J.; Pierce, N. A. A Unified Dynamic Programming Framework for the Analysis of Interacting Nucleic Acid Strands: Enhanced Models, Scalability, and Speed. *ACS Synth. Biol.* **2020**, *9* (10), 2665–2678. https://doi.org/10.1021/acssynbio.9b00523.

(38) Dirks, R. M.; Bois, J. S.; Schaeffer, J. M.; Winfree, E.; Pierce, N. A. Thermodynamic Analysis of Interacting Nucleic Acid Strands. *SIAM Rev.* **2007**, *49* (1), 65–88.

(39) Chen, Y.; Ma, H.; Duan, Y.; Ma, X.; Tan, L.; Dong, J.; Jin, C.; Wei, R. Mycobacterium Tuberculosis/Mycobacterium Bovis Triggered Different Variations in Lipid Composition of Bovine Alveolar Macrophages. *Sci. Rep.* **2022**, *12* (1), 13115. https://doi.org/10.1038/s41598-022-17531-2.

(40) Kolpashchikov, D. M. Binary Probes for Nucleic Acid Analysis. *Chem. Rev.* **2010**, *110* (8), 4709–4723. https://doi.org/10.1021/cr900323b.

(41) Mokany, E.; Tan, Y. L.; Bone, S. M.; Fuery, C. J.; Todd, A. V. MNAzyme QPCR with Superior Multiplexing Capacity. *Clin. Chem.* **2013**, *59* (2), 419–426. https://doi.org/10.1373/clinchem.2012.192930.

(42) Kuffel, A.; Gray, A.; Daeid, N. N. Impact of Metal Ions on PCR Inhibition and RT-PCR Efficiency. *Int. J. Legal Med.* **2021**, *135* (1), 63–72. https://doi.org/10.1007/s00414-020-02363-4.